DØNote 2767

Jet Production via Strongly-Interacting Color-Singlet Exchange in $p\bar{p}$ Collisions

(Supporting document for *Physical Review Letters* submission)

A. Brandt, B. May, T. Taylor
The DØ Collaboration

November 14, 1995

Abstract

A study of the particle multiplicity between jets with large rapidity separation has been performed using the DØ detector at the Fermilab Tevatron $p\bar{p}$ Collider operating at $\sqrt{s} = 1.8$ TeV. A significant excess of low-multiplicity events is observed above the expectation for single gluon/quark (color) exchange. The fractional excess is measured to be $(1.07 \pm 0.10(\text{stat})^{+0.25}_{-0.13}(\text{syst}))\%$, which is consistent with a strongly-interacting color-singlet exchange process and cannot be explained by electroweak exchange alone. A lower limit of 0.80% (95% C.L.) is obtained on the fraction of dijet events with color-singlet exchange, independent of the rapidity gap survival probability.

Introduction

In this note, we provide supporting documentation for the Physical Review Letters submission of September 20, 1995 (FERMILAB-PUB-95/302-E) with the same title as above. This is an updated analysis of the same data sample described in our first publication in Physical Review Letters [1], the dissertation of B. May [2], and conference DØNote 2579. Other proceedings with preliminary results related to this analysis are available as well, but are superseded by the present results. For this measurement we utilize particle multiplicity distributions measured in the calorimeter and tracking detectors to identify a color-singlet exchange signal.

In contrast with our previous results, which placed an upper limit on the fraction of color-singlet events, the goal of this analysis is to show definitive evidence for the existence of a signal at low particle multiplicity that is consistent with color-singlet exchange and inconsistent with color-exchange background. By measuring the value of the signal, it is possible to differentiate between a purely electroweak color singlet and a combination of electroweak and strongly-interacting color singlet. Outlined below is the approach taken in this analysis.

1. We motivate the use of the negative binomial distribution (NBD) as a reasonable parameterization for final-state particle multiplicity distributions in HEP reactions.

2. Using several Monte Carlo and data control samples, we show that particle (and calorimeter tower multiplicities) in jet events are well parameterized by a single NBD or superposition two of NBD's (double NBD). From this evidence, we postulate that the multiplicity between jets from color exchange is also well-described by a single or double NBD.

3. We also postulate (from theoretical arguments) that a color-singlet exchange signal would appear as an excess above the color-exchange expectation at low multiplicity. In order to show the existence of such a signal, however, we do not parameterize (or fit) the excess, as this could bias the results. Instead we fit only the part of the multiplicity distribution that can be well described by our color-exchange parameterization and extrapolate down to zero multiplicity to determine whether or not a signal is present and measure its value.

4. Once we have shown evidence for the existence of a signal (a statistically significant excess at low multiplicity) that is not explained by color exchange, we demonstrate that the signal is consistent with predictions for strongly-interacting color-singlet exchange.

5. Using the measured value for the excess, we place a lower limit on $\sigma_{\text{singlet}}/\sigma$, the fraction of dijet events due to color-singlet exchange, independent of the survival probability (the survival probability is discussed in Sec. 1).

6. Finally we show that an upward fluctuation of QCD color-exchange background plus a purely electroweak color singlet is very significantly excluded, which gives us further evidence for strongly-interacting color-singlet exchange.

This note elaborates fully on these analysis issues, although not necessarily in the same order as given above.

Part I
Theory and Background Fitting Method

1 Theoretical Motivation

The structure and topology of the final-state hadronic system in high transverse momentum $p\bar{p}$ interactions is typically interpreted in terms of final-state jets, which ideally correspond to the quarks and gluons participating in the hard interaction. However, a significant fraction of the final-state hadronic particle production occurs at large angles to the final-state jets. These particles cannot be associated with a unique hard parton (or jet), and their distribution is believed to be largely determined by the color flow of the hard partonic system.

Color flow and its effect on final-state particle production in $p\bar{p}$ collisions can be easily seen in the strikingly different particle production topologies of elastic and diffractive scattering compared to minimum bias events. In elastic or diffractive scattering, the proton and antiproton are believed to exchange a Pomeron, which has the quantum numbers of the vacuum. Since the Pomeron carries no color charge, there is no net color flow between the proton and antiproton. As a result, particle production is typically limited to small angles (from the beam axis). In elastic scattering, the final state consists of only the proton and antiproton (scattered at small angles), resulting in a large region in rapidity that is devoid of final-state particles. This region is called a rapidity gap.

Large rapidity gaps also arise in single and double diffraction due to the color-singlet nature of the Pomeron, although the size and location of the gap can vary depending on the kinematics of the collision. In contrast, $p\bar{p}$ minimum bias events do not have large rapidity gaps since they typically result from the exchange of a soft gluon (color octet), which produces the well-known rapidity plateau (i.e. uniform final-state particle production in η-ϕ space). (See the thesis for a general discussion of diffraction, color flow and rapidity gaps.)

Rapidity gaps are are expected to occur between jets when a color singlet is exchanged between interacting partons [3, 4]. The exchange of an electroweak gauge boson (photon, $W^{\pm}$, or Z^{0}) is expected to give this topology (see Fig. 1). Fletcher and Stelzer have shown that the exchange of a photon between two quarks leads to a large suppression of gluon

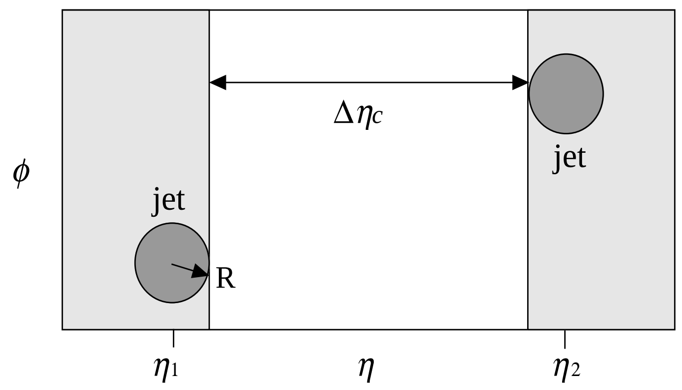

Figure 1: Representation in η-ϕ space of the distribution of particles in a two-jet event containing a rapidity gap. The pseudorapidity region between the edges of the jet cones, $\Delta\eta_c = |\eta_1 - \eta_2| - 2R$, contains no particles

radiation between the quark jets as compared to single gluon exchange[2, 5], resulting a region with few final-state particles. In addition, Chehime and Zeppenfeld have shown that the exchange of two gluons in a color-singlet state results in highly suppressed gluon radiation between two quarks, similar to photon exchange[2, 6]. This two-gluon color-singlet state has been proposed as a model for the QCD Pomeron [7, 8], although the true nature of the Pomeron remains unknown.

Bjorken [4] has estimated the fraction of events with color-singlet exchange to be roughly 10% using a two-gluon model for a QCD Pomeron. Del Duca and Tang [9] have also calculated the fraction and obtain a similar estimate using BFKL [8] theory. In contrast, the fraction for electroweak gauge boson exchange is calculated to be roughly 0.1% [10]. (See next section for Monte-Carlo calculation of the EW fraction). Thus a strongly-interacting color singlet is expected to dominate over photon, $W^{\pm}$, or Z^0 exchange.

Rapidity gaps (from any process) can be filled with final-state particles coming from interactions between spectator partons. The probability that there is no additional interaction between spectator partons (denoted $<|S|^2>$) has been estimated to be roughly 10% to 30% [4, 5, 11].[1] Thus, the fraction of events with an *observable* rapidity gap from

[1] We note a subtle point concerning the survival probability. The theorists calculate the probability of having no additional spectator interaction ($<|S|^2>$), which is not identical to the probability of having no particles from spectator interactions (S), since some portion of spectator interactions produce no particles within the region of interest. The latter quantity is what we are sensitive to experimentally, and the two

(two-gluon) Pomeron exchange is expected to be roughly 1–3%, while the fraction due to electroweak gauge boson exchange is about two orders of magnitude lower.

Although the exchange of a quark (color triplet) or gluon (color octet) typically produces particles between the jets, rapidity gaps can arise from fluctuations in the particle multiplicity. These gaps become highly suppressed as the rapidity interval between the jets increases [4, 10], but nonetheless are a background to color-singlet exchange that must be considered.

2 Calculation of Electroweak Color-Singlet Exchange

In this analysis, it is possible to differentiate between purely electroweak color-singlet exchange and strongly-interacting color-singlet exchange. In Ref. [10], the fraction of dijet events due to electroweak color-singlet exchange was calculated to be about 0.1% (7×10^{-4}) with a weak dependence on the η separation of the jets. However, as this calculation was done at leading order, higher-order radiative effects may modify the result. We therefore use the PYTHIA Monte Carlo [12] to determine this fraction, as the HERWIG Monte Carlo [13] does not currently implement the photon exchange sub-process, which is the dominant contributor to the electroweak dijet cross section. This approach has the benefit of allowing us to obtain the fraction for the E_T and η of the jets in our final data sample, as well as including the effects of higher-order gluon radiation.

Two samples of 100K events were generated, one with standard QCD matrix elements, and one with photon exchange. Both partons were required to have $p_T > 20$ GeV, with one parton having $\eta > 1.8$ and the other $\eta < -1.8$. The parton kinematic cuts were chosen to minimize any potential bias from turn-on effects. Jets were then reconstructed using the PJETS algorithm and a cut was made requiring the two highest E_T (leading) jets to have $|\eta| > 2.0$ and be on opposite sides in rapidity. The jet E_T efficiency was modelled and events were accepted on a statistical basis according to the turn-on curve. The turn-on curve was converted into a probability of the jet being accepted as a function of E_T. For each jet, a random number was generated and compared to the probability for a jet of that E_T being accepted. Both jets were required to be accepted for the event to be accepted.

quantities are equivalent within theoretical errors.

The fraction was then calculated according to the following equation

$$f_{\rm EW} = \frac{\sigma_{\rm EW}}{\sigma_{\rm dijet}} = \frac{\sigma_{\rm jj}^{\rm EW} \cdot N_{\rm acc}/N_{\rm gen}}{\sigma_{\rm jj}^{\rm QCD} \cdot N_{\rm acc}/N_{\rm gen}}$$

where the dijet cross sections were calculated by PYTHIA, $N_{\rm acc}$ was determined as described above, and $N_{\rm gen}$ is the number of generated events. A value of

$$f_{\rm EW} = (8.5 \pm 0.3) \times 10^{-4}$$

was obtained, where only the statistical error is given. The fraction was found to have little dependence on energy scale, ranging from 7.3—8.6 $\times\ 10^{-4}$ when the energy scale correction was varied by 1σ. The fraction also had very slight η dependence with no statistically significant change from varying the generated parton η in the range 1.6—2.0, or from requiring $\Delta\eta_c > 3.0$. No sensitivity was found to the level of spectator interactions. Turning off initial and final state radiation decreases the fraction by about a factor of 2, which is expected since QCD events tend to radiate more and would be relatively more likely to pass the E_T cuts with radiation turned off. We thus use $f_{\rm EW} = 9.0 \times 10^{-4}$, as the fraction of color-singlet events from EW exchange.

3 Published Results

First experimental results on the subject of hard diffraction were published by the UA8 Collaboration, which showed the existence of jets in single diffractive events [14] and that these jets had rapidity and longitudinal momentum distributions consistent with a hard pomeron structure [15]. There was also evidence for a "super-hard" or "coherent" pomeron, where the entire momentum of the pomeron participates in the hard scattering [15].

The UA8 Collaboration tagged diffractive events using a small angle spectrometer consisting of Roman pots to detect and reconstruct the leading proton or antiproton [16] and had acceptance for proton momentum transfers in the range $1 \lesssim |t| \lesssim 2$ GeV^2.

Diffractive jet production in *ep* collision at HERA was initially observed in DIS events with a large rapidity gap [17]. These jets are also well-described by the exchange of a pomeron with a hard structure. Recently, more extensive analysis has been done with jets produced in photoproduction (where a quasi-real $Q^2 \approx 0$ photon is exchanged) events with a large rapidity gap [18, 19]. These processes are dominated by low momentum transfer ($t \sim 0$) exchange.

The class of events studied here are markedly different, with a central rapidity gap as opposed to a forward one, and $|t| > 900\mathrm{GeV}^2$. The two previous publications on this subject are discussed below.

The DØ collaboration has previously reported a study of rapidity gaps between jets in PRL [1, 2]. In this study, the two highest transverse energy (E_T) jets were required to have $E_T > 30$ GeV, $|\eta| > 2$, and a separation of $\Delta\eta_c > 3$, where $\Delta\eta_c = |\eta_1 - \eta_2| - 1.4$ is the distance in η between the edges of the jet cones of radius 0.7 (see Fig. 1). Although rapidity gaps were observed with an experimental definition for a rapidity gap (i.e. no electromagnetic towers of $\Delta\eta \times \Delta\phi = 0.1 \times 0.1$ with more than 200 MeV), this did not directly imply observation of color-singlet exchange since inefficiencies could have created false gaps, and there was an indeterminate background from particle multiplicity fluctuations in color-exchange (gluon/quark exchange) events. An upper limit of 1.1% (at 95% C.L.) was placed on the fraction of events with a rapidity gap between the jets [1, 2], independent of the experimental definition of the rapidity gap. Although this measurement put a significant constraint on the rapidity gap fraction, it did not exclude a strongly-interacting color singlet.

The CDF Collaboration has measured the fraction of jet events with a rapidity gap using charged tracks with $p_T > 400$ MeV [20]. They also observed rapidity gaps (defined as the absence of tracks), but used a simple smooth fit to the rising part of the tracking multiplicity distribution to estimate the background from fluctuations. They quoted a fraction of $0.0085 \pm 0.0012(stat) + 0.0024(sys) - 0.0012(sys)$, which is consistent with the rough estimate for two-gluon Pomeron exchange, although it should be pointed out that (in our opinion) this measurement includes a spectator interaction contribution to the zero track multiplicity, and is thus not a measurement of the rapidity gap fraction.

4 Theoretical Motivation for Multiplicity Measurement

The final-state particle multiplicity distribution between jets offers a convenient way to search for color-singlet exchange. Naively, color-singlet exchange is expected to give zero multiplicity between jets (i.e. a clear rapidity gap) for events that do not have an additional (spectator) interaction [4]. For those events that do not "survive" spectator interactions, the multiplicity distribution is expected to be similar to that in minimum bias events [21, 22]. Therefore, for color-singlet exchange events, the multiplicity is naively expected to have a component at zero multiplicity of $<|S|^2>\cdot\sigma_{\rm singlet}$, while $(1-<|S|^2>)\sigma_{\rm singlet}$ is distributed in a minimum-bias-like distribution (see Ref. [23] for an example of minimum bias multiplicity distributions).

However, this naive picture ignores the effects of jet fragmentation (called out-of-cone radiation), which can result in particles associated with the jets spilling into the gap (see thesis for discussion). Since a finite jet cone will not always contain all particles from a jet, the multiplicity of the "surviving" color-singlet rapidity gaps will be smeared to non-zero but low multiplicity. In addition, the multiplicity of the "non-surviving" (i.e. events with spectator interactions) rapidity gap events will be increased slightly to a higher multiplicity, but this effect is not as significant to the measurement as the effect on the surviving rapidity gap events.

Unlike color-singlet exchange, the exchange of a quark (color triplet) or gluon (color octet) is expected to give a large mean multiplicity between jets due to the color flow in these interactions, and the multiplicity distribution is naively expected to have a negative binomial (or similar) multiplicity distribution [24]. In addition, the mean multiplicity between jets is expected to increase as the rapidity separation between the jets increases due to the increased phase space (η-ϕ space) for particle production [4].

Therefore, due to the distinctly different multiplicity distributions for color-singlet exchange versus color (quark/gluon) exchange, it should be possible to distinguish the two by measuring the particle multiplicity between jets. An excess of low multiplicity events compared to the expectation for the color-exchange background would indicate the presence of color-singlet exchange. It is therefore crucial to understand the shape of the multiplicity distribution for color exchange.

A historically successful parameterization for particle multiplicity distributions in HEP is the negative binomial distribution. The following sections describe the experimental and theoretical motivation for the negative binomial distribution as a parameterization for final-state particle multiplicity distributions.

NBD and High-Energy Multiplicity Distributions

The negative binomial distribution (or NBD) has been used extensively (and successfully) as a parameterization for various particle multiplicity measurements in high energy collisions, ranging from fixed target to DIS, e^+e^- and $p\bar{p}$ collider experiments [23, 25]. The NBD has been phenomenologically successful in fitting charged particle multiplicity distributions in full phase space and in symmetric rapidity intervals about $\eta = 0$ in hadron-hadron collisions, as well as in other types of high-energy reactions, including e^+e^- collisions.

Interestingly, in higher center-of-mass energy collisions (in $p\bar{p}$ collisions at $\sqrt{s} = 900 - 1800\,\mathrm{GeV}$ and in e^+e^- collisions at $\sqrt{s} = 91\,\mathrm{GeV}$), a single NBD does not fit the experimental charged particle multiplicity distributions well, due to the development of a high multiplicity "shoulder" that effectively widens the distributions. In e^+e^- reactions, this has been interpreted as the superposition of different topologies (or interactions) each of which have an underlying NBD [25]. In $p\bar{p}$ collisions, this shoulder is interpreted as the onset of a semi-hard component arising from an increasing "minijet" contribution to the minimum bias cross-section [26, 27]. Therefore, at present most charged particle multiplicity distributions in high-energy reactions have been successfully fit by either a single NBD or a superposition of NBD's, which presumably accounts for additional independent sources of final-state charged particles. (For an overview of multiplicity distributions in high-energy collisions, see Refs. [28], [29] and [30].)

Multiplicity between Jets in e^+e^-

Although the NBD has been successful in fitting multiplicities from various high energy processes, particle multiplicities in e^+e^- can effectively provide a measurement of the "QCD background" multiplicity between jets. That is, particle production between jets as measured in e^+e^- experiments, can provide a qualitative picture of QCD radiation between jets in $p\bar{p}$ collisions with color exchange. While the values of the parameters of the multiplicity distributions are not expected to be the same as in $p\bar{p}$ jet events, the qualitative features should be universal, since final-state fragmentation of jets is believed to be universal.

The DELPHI collaboration [25] has published data on charged particle multiplicity in jet events. The total event multiplicity (including the jets) has been shown to deviate from a NBD, but this is believed to be due to the different multiplicity distributions from two-jet and multijet (three or more) events. However, plotting multiplicity distributions versus a fixed number of jets leads to distributions that are more consistent with a NBD.

The DELPHI collaboration has measured the multiplicity in various rapidity regions (as defined by the thrust axis) for various numbers of jets in the event. For two-jet events, this is equivalent to measuring the multiplicity between the jets, as a function of the allowed rapidity interval ($|y| < 0.5, 1.0, 1.5, 2.0$). For each of these regions, *the multiplicity is consistent with a NBD.* More importantly, there is no deviation (or excess) at low particle multiplicity, indicating that final-state QCD radiation (and subsequent hadronization) leads to a smooth multiplicity distribution between jets that is consistent with a negative binomial parameterization. Therefore, e^+e^- data suggests that the NBD is a reasonable candidate parameterization for multiplicities between jets in $p\bar{p}$, although it is possible that a superposition of NBD's may be needed to account for the multiple subprocesses that contribute to jet production in $p\bar{p}$ collisions.

Theoretical Basis for NBD

Although the NBD has been successfully used to fit experimental multiplicity distributions, the physical origin or justification for such a distribution remains somewhat elusive. Various physically motivated models for final-state particle production have resulted in a NBD (or very similar distributions), but these models assume simple processes, and the underlying assumptions cannot at present be tested experimentally. One model that reproduces a NBD is based on a simple cascade or fragmentation type mechanism which implement a two-stage process for final-state particle production[30]. In the first stage, clusters are formed according to a Poisson distribution. In the second stage, each cluster decays into final-state hadrons according to a logarithmic distribution. The convolution of these processes leads to a NBD[30]. Varying the cluster decay distribution from a logarithmic distribution, has been shown not to affect significantly the shape of the final multiplicity distribution [31]. Other models also have been proposed which lead to a negative binomial (or very similar) distribution [30].

Multiplicity distributions (at the parton level) have also been calculated within perturbative QCD[28, 32, 33, 34]. In these calculations, leading logs are summed to determine the parton multiplicity in jets. Assuming local parton-hadron duality, the resulting multiplicity distributions are very similar to a NBD, and contain properties that are consistent with multiplicities observed in e^+e^- data. However, some qualitative differences do exist as seen in higher-order moment analysis. Nevertheless, even though the NBD may not be the exact answer, for most purposes it provides an excellent parameterization for particle multiplicity in high energy reactions.

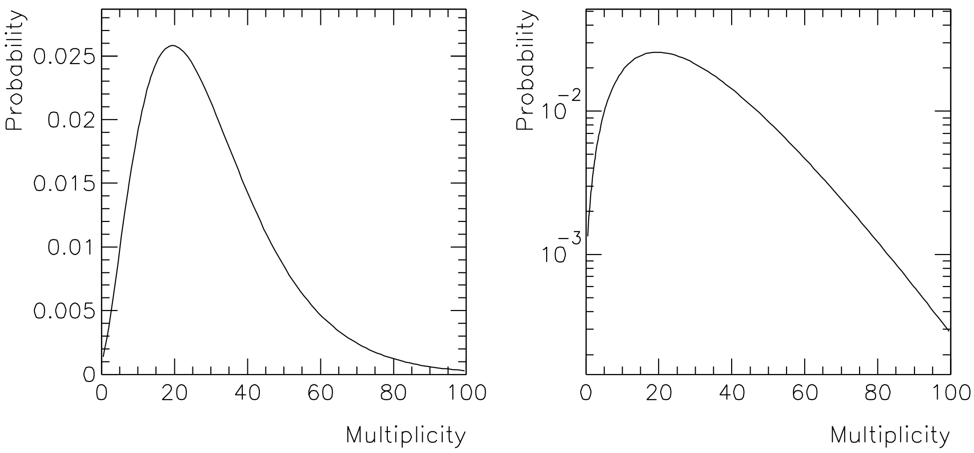

Figure 2: Example of a NB distribution shown on linear and log scales.

Properties of NBD

The NBD has the following form:

$$P(n) \quad = \quad \binom{n+k-1}{k-1}\left(\frac{\bar{n}}{k+\bar{n}}\right)^n \frac{1}{(1+\bar{n}/k)^k}$$

where n is the particle multiplicity, $\bar{n}$ is the average particle multiplicity, and k is a measure of the distribution width. The variance of the distribution D^2 is related to k by $k^{-1} = D^2/\bar{n}^2 - 1/\bar{n}$. The mode (maximum value) of the NBD is given by $n_{mode} \approx \bar{n}(1-1/k)$. As shown in Fig. 2, the NBD thus has the following qualitative behavior (for $\bar{n} \gg k > 1$): a smooth (exponential-like) rise from small values to a peak near but below the mean value and then a long (exponential-like) tail out to higher n.

The NBD reduces to several well-known distributions in certain limits. For $k = 1$, the NBD reduces to a Bose-Einstein distribution, while for $k \to \infty$, it reduces to a Poisson distribution. For fixed k and $n \gg k$, the NBD can be approximated by a Gamma distribution. In fact, the NBD is equivalent to a Gamma distribution convoluted with a binomial distribution. Thus, if the underlying full particle multiplicity distribution is a Gamma distribution, both charged and neutral multiplicity distributions should have a NBD form.

Other Parameterizations

The NBD is not the only successful parameterization used to fit multiplicity distributions. Although other parameterizations lead to comparable fits, no single parameterization has been shown to fit the experimental distributions significantly better than the NBD [30, 31]. It is interesting to note that most of the successful parameterizations have the general form of a compound Poisson distribution [30], which assumes an underlying Poisson distribution for "clusters" convoluted with a distribution that describes the "decay" multiplicity. The resulting distributions are similar, leading to the conclusion that the specific details of the process are perhaps not as important as the fact that it is a two-step process. Therefore, the phenomenological success of the NBD is not a proof that the underlying distributions are truly of a negative binomial form, but perhaps an indication that the exact form is not very critical, as long as it is consistent with the data.

Clearly it is useful to try other reasonable parameterizations, to see how sensitive the results are to the specific choice of parameterization, however, due to the success of the NBD in this particular analysis (almost all other distributions we have tried can be excluded), the NBD (and double NBD) will be the standard parameterization used in this analysis.

5 Method for Multiplicity Measurement

In order to measure an excess at low multiplicity in our data samples, we use a parameterization of the color-exchange multiplicity to extrapolate down to low multiplicity. Any difference between the extrapolation (color-exchange background) and the data would therefore be a measure of a color-singlet signal. The logical argument for the analysis method is as follows:

1. We postulate that the color-exchange multiplicity distribution is parameterized well with a single or double NBD, i.e. the color-exchange multiplicity distribution is a smoothly rising and falling distribution with no anomalous deviations (excesses or bumps) from the smooth form.

   We test the NBD hypothesis by looking at the multiplicity in several complementary "control" samples (which have detector effects included):

   (a) Several Monte Carlo samples, which provide a rough theoretical prediction for the multiplicity between jets in color-exchange events (Sec. 6).

(b) A large sample of "same-side" events, which provides a sample of color-exchange like multiplicity (Sec. 7).
(c) A color-exchange subsample (color-singlet suppressed) consisting of color-exchange events that have a jet between the two leading E_T jets. This sample should have the qualitative features of an inclusive color-exchange sample. (Sec. 7).

We test the overall quality of the fits to the control samples and also try to measure a signal in these samples using the same method used on the data. If the control samples are parameterized reasonably well by the NBD and do not have a significant signal at low multiplicity, then this supports the NBD hypothesis.

2. Assuming a NBD, we test our method of fitting and extrapolating and its ability to measure a low multiplicity excess. This is done on a large ensemble of NBD Monte Carlo distributions and on the control samples. We check that the fits (excluding the low multiplicity bins) are not biased and give a reliable extrapolation to low multiplicity bins. We also test the method of measuring a signal on these MC distributions to show that the probability of fluctuations producing a false signal is small.

3. With the support above, we hypothesize that the color-exchange background is well-modeled by the NBD. We fit the data excluding low multiplicity bins (as determined by the adaptive fitting method) and extrapolate the fit down to zero multiplicity. The fit is used to obtain an unbiased measure of the excess above the color-exchange background in the low multiplicity bins.

   Since we wish first to determine if there is a signal and second to measure its value, we do not parameterize the signal as this could bias the result. Instead we employ an adaptive fitting method that determines the lowest starting multiplicity bin for which the fit to the background (from that multiplicity bin on) becomes "good". Thus if there were a statistically significant signal at low multiplicity, this method would find the first multiplicity (bin) in which the signal becomes statistically "small". The fit is then extrapolated down to zero multiplicity, and the difference between the data and fit (i.e. the excess above the parameterization) is used to measure the signal.

4. We verify the "signal" with the tracking detector, which provides an independent confirmation of the excess.

5. We use a conservative value of the excess with appropriate errors in order to place a lower limit on the signal. This lower limit can be used directly to place a lower limit on the ratio $\sigma_{\mathrm{singlet}}/\sigma$.

Using this method it is possible to determine a lower limit that, independent of the experimental multiplicity distribution, can be compared to our previously published upper limit and directly to the theoretical predictions for $\sigma_{\mathrm{singlet}}/\sigma$.

Fitting Considerations

There are generally two widely accepted methods for determining the "best" fit parameters to a distribution. The χ^2 method uses an effective least squares method and assumes Gaussian errors, while the maximum likelihood method maximizes the log likelihood function which assumes Poisson errors. For histograms in which all bins have a large number of events, the two methods give essentially identical results. However, the χ^2 method can give significantly biased values for the fit parameter values if the distribution has bins with few events. The maximum likelihood method is believed to give unbiased estimates for the parameters, if unbiased estimators exist.

Another concern with fitting distributions is the goodness-of-fit. The most widely accepted goodness of fit measure is the χ^2/df. Although the χ^2/df gives an indication of the goodness-of-fit, it is generally only useful for excluding fits above a certain confidence level. It is perhaps useful to note that the power of the χ^2 test can be affected by bin size, and it is important to vary the binning to see if it significantly changes the confidence level for a fit. If any one χ^2 test on the fit very significantly excludes the fit, then the fit is excluded even if other χ^2 values are good.

In conjunction with the χ^2 goodness-of-fit, we have developed an additional test that is more sensitive to systematic deviations or shape differences. The Kolmogorov-Smirnov test [35], uses various measures to test the difference between the cumulative distribution of the fit and the data. The cumulative distribution is useful because it tends to be sensitive to systematic shape differences that are not obvious in comparing differential distributions. The so-called Kolmogorov-Smirnov (K-S) statistic is the maximum value of the absolute difference between the the cumulative distributions. This statistic is most sensitive to differences in the middle of the distributions and is not as sensitive to differences in the tails. We have developed an additional statistic based on the integrated square difference (area) between the two cumulative distributions, which is sensitive to the overall systematic differences. We use this statistic (in addition to χ^2) to determine the relative goodness of the fits to the data.

Once a parameterization has been shown to have a reasonable goodness-of-fit, it is necessary to show that there are no systematic deviations or effects at low multiplicity. We therefore test the adaptive fitting method on a sample of simulated NBD's (and our control samples) in order to determine if the extrapolation to low multiplicity provides a reliable estimator of the low multiplicity distribution. In this way, it can be shown that the parameterization is a sufficient model for the background at low multiplicity.

Adaptive Fitting Method

In order to measure any low multiplicity excess or signal in an unbiased way, we have developed an adaptive fitting method which determines the lowest multiplicity bin at which the fit to the multiplicity distribution (from that multiplicity bin on) becomes "good". The fit is then extrapolated down to zero multiplicity, and the difference between the distribution and fit (i.e. the excess above the parameterization) is used to measure the "signal".

The goodness-of-fit measure to determine the starting point (n_0) for the fits is given by:

$$\chi_5^2(n_0) \quad = \quad \frac{1}{5}\sum_{n=n_0}^{n_0+5} \frac{(N_{\rm data}(n) - N_{\rm fit}(n))^2}{N_{\rm data}(n)}$$

If $\chi_5^2(n_0)$ shows statistically significant deviations in the first few bins of the fit, the starting point of the fit (n_0) is incremented by one unit in multiplicity, the fit is redone starting from the new n_0, and $\chi_5^2(n_0)$ is recalculated. The first starting point for which $\chi_5^2(n_0) < 2.0$ (no statistically significant deviation) is taken as the lowest acceptable starting point for the fit.

Clearly, for samples in which no signal is expected (such as the control samples or the NBD MC samples), the adaptive fitting method should give no (or very a small) excess: that is, the fit should start at multiplicity close to zero (first bin) and any excess should not be statistically significant. In contrast, a statistically significant signal is expected in the inclusive opposite-side dijet sample if there is a significant color-singlet signal.

Measurement of Excess at Low Multiplicity

The *fractional integrated excess* at low multiplicity measured with respect to a given color-exchange background distribution $N_{\rm NBD}(n)$ is given by

$$f(n_0) = \frac{\sum_{n=0}^{n_0}(N_{\rm data}(n) - N_{\rm NBD}(n))}{N_{\rm total}}. \quad (1)$$

The background distribution is generally obtained by fitting some portion of the distribution $N_{\rm data}(n)$. We define three quantities, each using a different reference distribution, as a measure of the low multiplicity excess:

1. If the exact underlying multiplicity distribution is known (as in a simple Monte Carlo generator), the difference between the generated "data" histogram and the underlying multiplicity distribution is called the exact excess. The standard deviation of the exact excess is identical to purely statistical error of the excess.

2. If the multiplicity distribution $N_{\rm data}(n)$ is fit over its entire range to obtain $N_{\rm NBD}(n)$, the difference between the data and the fit is called the nominal excess.

3. If the multiplicity distribution $N_{\rm data}(n)$ is fit starting from a non-zero multiplicity ($n > 0$) to obtain $N_{\rm NBD}(n)$, the difference between the data and the fit is called the extrapolated excess.

The extrapolated excess is the only measure not biased by a true excess at low multiplicity. However, each method should give results consistent with zero (although with different errors) fitting to distributions in which no low multiplicity excess is actually present.

Fitting Tests on a NB Monte-Carlo

We have written a Monte Carlo program to generate ensembles of NB distributions with the same parameter values in order to obtain distributions of the goodness-of-fit statistics, test the appropriateness of the adaptive fitting method, and determine if the extrapolation procedure is reliable. The parameters of the NBD's in the ensembles ($\bar{n}$, k, and number of events) were chosen to be close to those obtained from the data, but the results are not very sensitive to reasonable variations in the parameters.

Although the χ^2 fitting method had initially been used to determine the fit parameters and evaluate the fits (as in DØNote 2579), this method has since been shown to produce biased values for the fit parameters, i.e. the parameters obtained from the χ^2 method were systematically biased away from the actual parameters used to generate the Monte Carlo ensemble. This is most likely due to the bins in the tails of the distributions which had small statistics. The χ^2 method also produced a small but significant (undesirable) systematic excess at low multiplicity due to this bias. In contrast, the maximum likelihood method gave consistent and unbiased results for the fit parameter values. We therefore use this method to obtain the fits and determine if an artificial excess is generated by the fitting and extrapolating procedure.

We used a single and double NBD parameterization to test the sensitivity of the methods. We generated two ensembles of 500 Monte Carlo distributions with 15,000 events each. The single NBD ensemble was generated with the parameters $\bar{n} = 28$ and $k = 3.2$, which are typical for fits to the data. The double NBD ensemble had the parameters $\bar{n}_1 = 27$, $k_1 = 3.0$, $\bar{n}_2 = 29$, $k_2 = 5.0$, which assumes a relative normalization of 0.5 for each NBD.

Using the MC NBD ensembles, we tested the adaptive fitting and extrapolation procedures as follows:

1. The distributions in the ensemble are fit with the appropriate NBD (single or double). For each fit, various measures of the goodness-of-fit are determined, including χ^2/df, χ^2/df for larger bin sizes (more sensitive to shape differences), and the K-S statistic. The value of χ_5^2 is also determined. The distribution of χ_5^2 is used to determine a suitable value to cut on that is insensitive to statistical fluctuations at the beginning of the fits. This value will then be used on the control samples and the data to determine the starting point of each fit and determine if there is a statistically significant signal.

2. The starting point n_0 of the fit is incremented by one and the fits are redone. The exact, nominal and extrapolated fractional integrated excess (as defined above) are calculated in order to measure the low multiplicity excess in the multiplicity region $0 \leq n < n_0$. The value of χ_5^2 is also redetermined.

3. Step 2 is repeated for $0 \leq n_0 \leq 6$.

The mean exact, nominal and extrapolated fractional integrated excess for both ensembles were determined to be negligible for $0 \leq n_0 \leq 6$ (i.e. $|f(n_0)| < 0.02\%$). This affirms that the fitting method (using maximum likelihood) does not bias the extrapolation to low multiplicity and cause a systematic excess. However, the excess obtained on a distribution-by-distribution basis does fluctuate due to the limited statistics at low multiplicity and the errors in extrapolating to low multiplicity. The standard deviation of the measured excess is shown in Table 1. Interestingly, the standard deviation of the nominal (full fit) excess is smaller than the statistical error (s.d. on exact excess). This is not surprising since fitting down to low multiplicity bins would reduce the excess measured in those bins. In contrast, the extrapolated excess is subject to larger fluctuations since the low multiplicity bins are excluded from the fit. As n_0 increases, the error grows roughly linearly.

	Single NBD			Double NBD		
Start bin	Exact	Nominal	Extrap.	Exact	Nominal	Extrap.
$n_0 = 0$	0.02	0.02	0.02	0.04	0.04	0.04
$n_0 = 2$	0.06	0.06	0.07	0.11	0.09	0.11
$n_0 = 4$	0.12	0.09	0.13	0.18	0.13	0.22
$n_0 = 6$	0.17	0.12	0.22	0.24	0.15	0.40

Table 1: The standard deviation of the fractional excess $f(n_0)$ (in %) obtained from fits to the NBD Monte Carlo ensembles.

As mentioned above, the adaptive fitting method searches for a starting point of the fit based on the goodness-of-fit at the beginning of the fit (χ^2_5). We wish to choose a cut value such that typically no excess is found in the MC distributions. If, however, an excess is found, it should be small. Figure 3 shows the low multiplicity excess obtained using $\chi^2_5 < 2$ for the single NBD fits. Less than 1% of the distributions have an excess greater than 0.2%.

From the results discussed above, it is clear that the fitting and extrapolating method produces no significant bias at low multiplicity (assuming either a single or double NBD and fitting appropriately), but is subject to fluctuations that increase with n_0. However, implementing a suitable adaptive fitting method shows that actually finding a low multiplicity excess on a distribution by distribution basis is rare and the value of any excess is small.

6 Monte Carlo Color-Exchange Multiplicity

Several Monte Carlo studies were done to test the NBD hypothesis for the multiplicity between jets in color-exchange events. A PYTHIA 5.6 [12] Monte Carlo study (done by Fletcher) of color-exchange events using similar jet requirements as the DØ analysis (in-

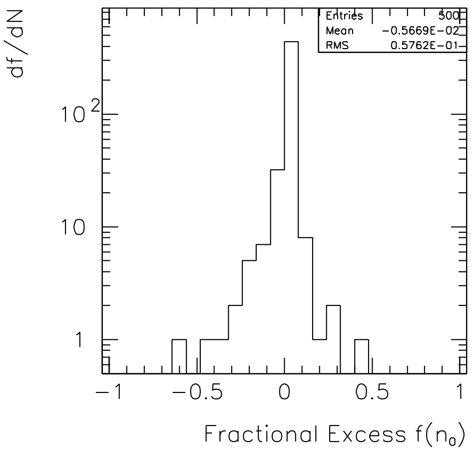

Figure 3: The excess (in %) found using the adaptive fitting method with a cut of $\chi^2_5 < 2$ on the single NBD MC ensemble.

cluding estimated DØ acceptance and efficiencies) yields a multiplicity distribution that is reasonably well-described by a single NBD [21]. A comparable study (done by Pumplin) using HERWIG [13] shows similar behavior, although a very small ($< 0.2\%$) excess at low multiplicity was observed in a very high statistics run [36]. In addition, in the HERWIG study, the sum of two NBD's fit the distributions better than a single NBD, although for event samples with less than 50K events, a single NBD gave a reasonable fit.

For completeness, we have performed our own simulation using PYTHIA 5.6. This sample was generated by requiring two jets at the parton level, each with $E_T > 25\,\mathrm{GeV}$ and $|\eta| > 1.8$, with an additional requirement that the jets be at opposite $|\eta|$. At the PJET level, the two highest E_T jets were required to have $E_T > 30\,\mathrm{GeV}$, $|\eta| > 2.0$ and $\Delta\eta_{jj} > 4.0$ ($\Delta\eta_c > 2.6$), resulting in about 20K events. These PJET conditions simulate the acceptance of the high-$\Delta\eta_c$ trigger which is used to search for a rapidity gap signal.

These events were used to investigate the multiplicity distributions between jets for several pseudorapidity regions and for various particle p_T thresholds in order to simulate acceptance effects and particle detection efficiency respectively. Five pseudorapidity regions between the jets were used: $\Delta\eta = 2$ (i.e. $|\eta_{particle}| < 1$), $\Delta\eta = 2.6$, $\Delta\eta_c > 3$, $\Delta\eta_c > 3.5$, $\Delta\eta_c > 4$. The first two regions are independent of the jet cone edges and simulate the acceptance of the central calorimeter or CDC, while the $\Delta\eta_c$ regions depend on the jet location. In addition, five particle p_T thresholds were used to count particle multiplicities: no cut, 100 MeV, 200 MeV, 300 MeV and 500 MeV. Figure 4 shows the multiplicity distribution (with single NBD fits) for the five pseudorapidity regions for all particles (no p_T cut). Figure 5 shows the multiplicity distribution (with single NBD fits) for the various p_T thresholds for $\Delta\eta = 2$. The multiplicity distributions have the expected qualitative shape consistent with a NBD: a smooth rise from small values (no excess or bump) to a peak near the mean value and then a long tail out to higher multiplicities.

Although single NBD fits to the distributions are typically not very good ($0.7 < \chi^2/df < 3.0$), qualitatively the distributions are not significantly different than the NBD fits and there is no excess at low multiplicity. This is an interesting result because all of the computational complexities of the Monte Carlo (i.e. the LO subprocess + parton showering + angular ordering + string fragmentation) reduce to a multiplicity distribution between the jets that is qualitatively very similar to a NBD. It is unlikely that this is a fortuitous result: the NBD parameterization (and/or superposition of several NBD's) has been successful in fitting many particle multiplicity distributions. However, it is perhaps surprising that the MC multiplicity is so NBD-like, since this distribution is not explicitly simulated but is the result of all of the approximations that go into the simulation.

Despite the qualitative success of a single NBD, fits to a double NBD give significantly better χ^2/df. Table 2 shows the respective χ^2/df and confidence levels for the two fits for several pseudorapidity regions and particle p_T thresholds. The double NBD fits to the distributions give no significant excess at low multiplicity. In addition, applying the adaptive fitting method to the distributions yields a null excess (i.e. $\chi^2_5 < 2$).

		Single NBD		Double NBD		Nominal Excess (%)	
Region	Threshold	χ^2/df	C.L.	χ^2/df	C.L.	$f(n_0 = 2)$	$f(n_0 = 4)$
$\Delta\eta = 2.0$	$p_T > 0.0$ GeV	1.44	0.3%	1.15	15.3%	2.1×10^{-3}	-6.7×10^{-2}
$\Delta\eta = 2.0$	$p_T > 0.2$ GeV	1.80	0.004%	0.93	64.7%	-5.4×10^{-2}	-6.4×10^{-2}
$\Delta\eta_c > 3.0$	$p_T > 0.0$ GeV	1.27	4.0%	1.22	8.2%	-2.6×10^{-4}	-2.2×10^{-3}
$\Delta\eta_c > 3.0$	$p_T > 0.2$ GeV	1.03	41.3%	0.91	71.9%	-7.7×10^{-3}	-3.0×10^{-2}

Table 2: Comparison of single and double NBD fits to multiplicity distributions from PYTHIA for a few pseudorapidity regions and particle p_T thresholds.

One possible explanation for the inconsistency of the multiplicity distribution with a

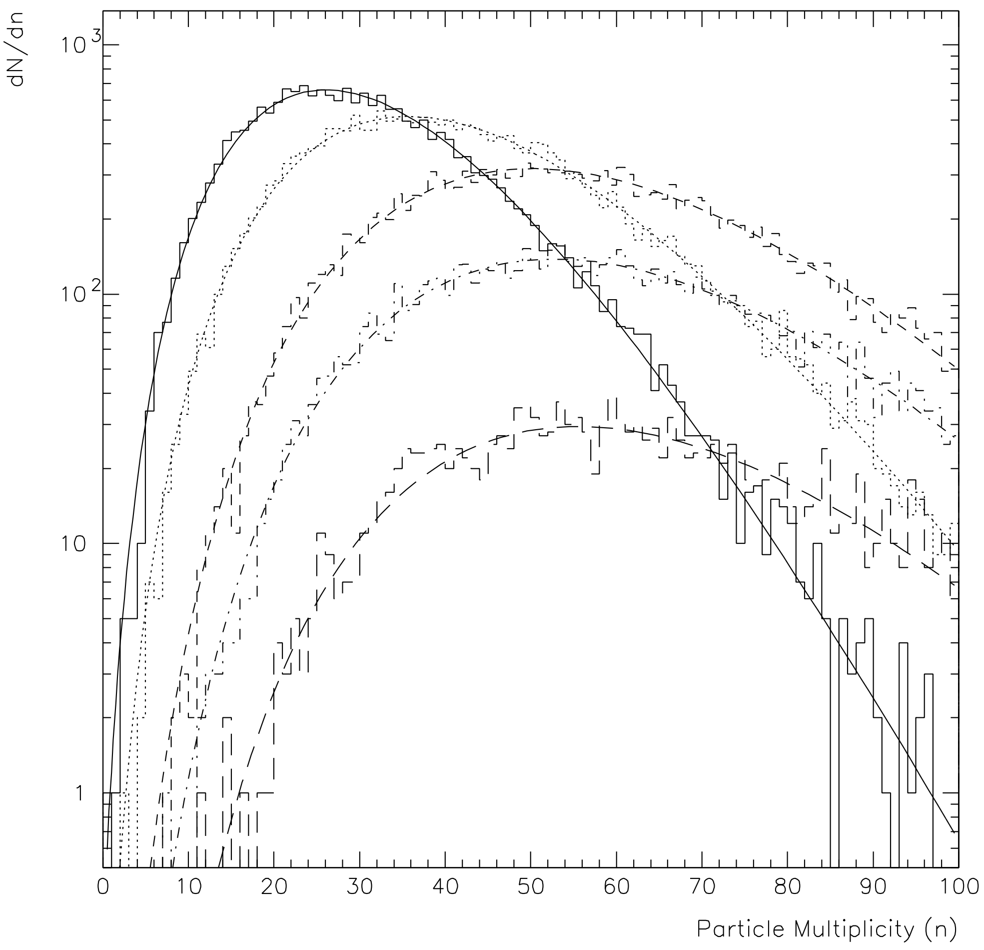

Figure 4: Particle multiplicity distributions (with single NBD fits) from PYTHIA for the five pseudorapidity regions discussed in the text. The average multiplicity increases with the size of the region.

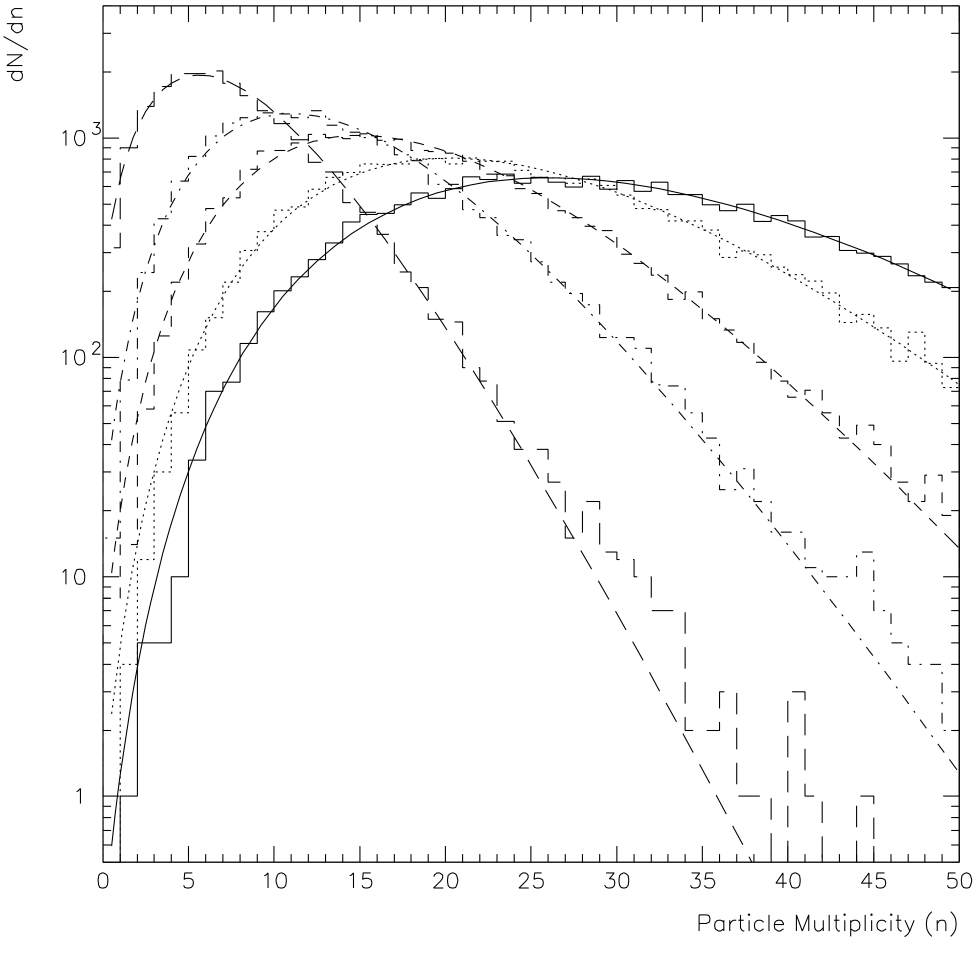

Figure 5: Particle multiplicity distributions (with single NBD fits) from PYTHIA for the five p_T thresholds discussed in the text. The average multiplicity decreases as the p_T threshold is increased.

single NBD is that three main subprocesses contribute to the sample of dijet events: $qq \to qq$, $qg \to qg$, and $gg \to gg$ which were in the ratio 1.0:1.3:0.5. As the $\Delta\eta_c$ is increased from 2.6 to 3.5, the ratio becomes 1.0:1.0:0.3. Therefore, for events that satisfy our DØ high-$\Delta\eta_c$ trigger conditions, two subprocesses dominate the cross-section. This is an important point since the final-state particle multiplicity distributions between the jets for the three subprocesses are significantly different (different means and widths) as shown in Fig. 6. This is most likely due to differences in the parton showering for the three final states, as turning off initial and final state parton showering (string fragmentation only) gives multiplicity distributions that are very similar for each process.

The single NBD fits to the multiplicity distributions for each subprocess are slightly better (although not significantly) than the fits to the inclusive multiplicity distributions. The success of the double NBD fits (as opposed the the single NBD) to the inclusive multiplicity distribution is perhaps partially explained then by the contribution of the two subprocesses $qq \to qq$ and $qg \to qg$. Therefore it is possible that double NBD fits might be necessary in the data as well.

PYTHIA+GEANT simulation

We have also performed a simulation using PYTHIA and the full DØ detector GEANT simulation [37]. This sample was generated by requiring that the scattered partons each have $E_T > 25\,\text{GeV}$ and $|\eta| > 1.6$, with an additional requirement that the jets be on opposite sides in η. At the PJET level, the two highest E_T jets were required to have $E_T > 30\,\text{GeV}$, $|\eta| > 2.0$ and $\Delta\eta > 4.0$, resulting in 3742 events. In order to reduce the simulation time for these events, only the particles with $|\eta| < 1.3$ were kept. The events were subsequently put through GEANT and RECO 12.15 in order to determine the multiplicity of electromagnetic calorimeter towers between the jets (see Sec. 8).

Figure 7 shows the multiplicity of EM towers ($E_T > 200$ MeV) in the rapidity interval $|\eta| < 1$ ($\Delta\eta = 2$). Although the parameters of the distribution are significantly different than the parameters obtained from the data, the NBD gives a good fit after detector simulation, with no significant excess at the low multiplicity. The results of the fit are given in Table 3. There are insufficient statistics to fit a double NBD, and a larger sample is currently being simulated. The excellent fit in this color-exchange sample is further support for the NBD parameterization method and indicates that there is no instrumentally produced

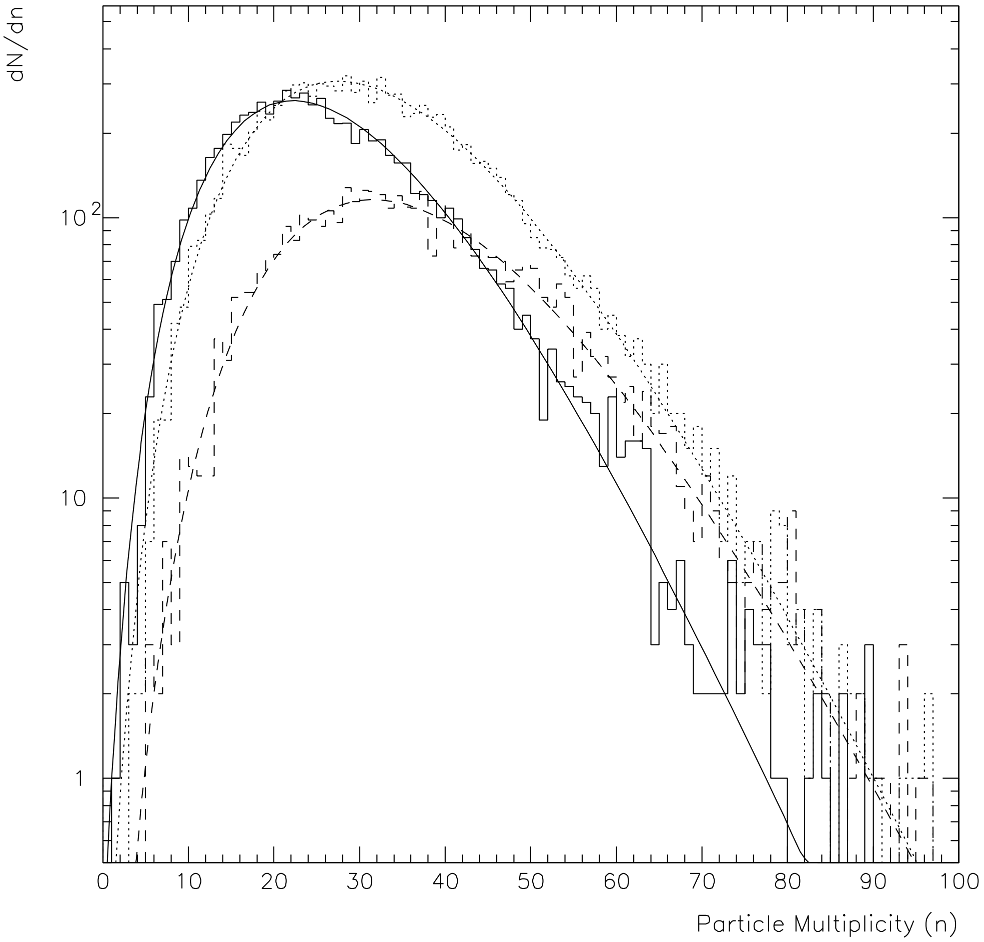

Figure 6: Particle multiplicity distributions (with single NBD fits) for the three primary subprocesses contributing to the total multiplicity distribution. The qq final state (solid curve) has the smallest mean multiplicity, the qg final state has intermediate multiplicity (dotted curve), and the gg process has the largest multiplicity.

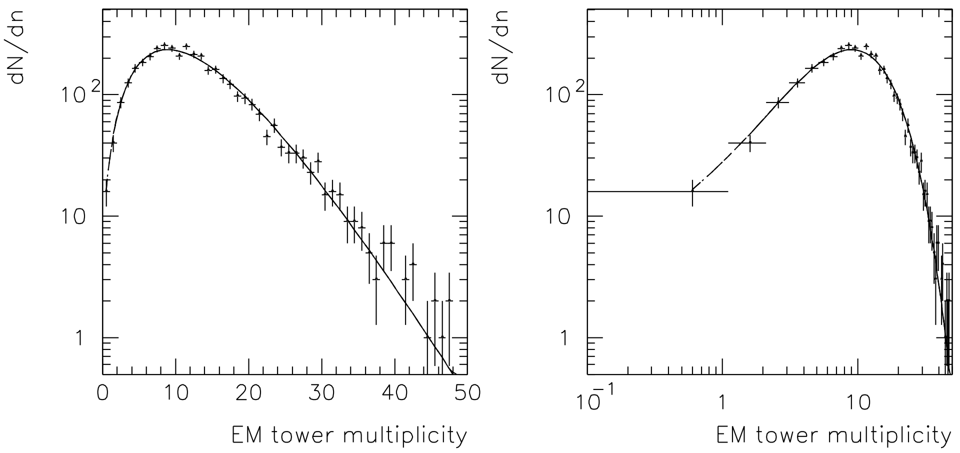

Figure 7: (a) The calorimeter tower multiplicity distribution in the region $|\eta| < 1$ for a sample of PYTHIA color-exchange events after full detector simulation. The solid line is a single NBD fit to the Monte Carlo sample. (b) shows a log-log version of the same plot.

excess.

χ^2/df	C.L.	χ_5^2/df	C.L.	$f(n_0)$	$f(1)$ (%)
0.85	75%	0.3	88%	0	-0.0002 ± 0.002

Table 3: NBD fit to the opposite-side color-exchange sample after full detector simulation for $\Delta\eta = 2$. The multiplicity distribution is fit using ($n_0 = 0$) since $\chi_5^2 < 2$. Shown is χ^2/df and associated confidence level (C.L.), χ_5^2 and associated C.L., the fractional excess above the fit for $n < n_0$ ($f(n_0)$), and the fractional excess $f(1)$ (in %) when the fit is forced to start at $n_0 = 1$.

Part II

Evidence for Color-Singlet Exchange

7 Triggers and Data Selection

This analysis primarily utilizes "high-$\Delta\eta_c$" Run-1a trigger JET_GAP_MED described in the first rapidity gap PRL [1] and the accompanying dissertation [2]. This trigger was implemented in order to maximize statistics for events with large rapidity separation between jets and is used to search for rapidity gap events and color-singlet exchange. The specific requirements for this "opposite-side" trigger and resulting statistics are summarized in Table 4. Note that there are no requirements on energy or multiplicity between the jets which would bias the fraction of events with a rapidity gap.

A sample of events with both jets on the "same side" (in rapidity) of the detector is useful for qualitatively modeling the color-exchange background in the central region of the detector. Any rapidity gaps from a color-singlet component of these events would be between the jets in the forward region, while the multiplicity in the central region would be expected to be characteristic of color-exchange (due to the color string between the scattered and spectator partons). Furthermore, any hard single diffractive component, which could produce a central rapidity gap and same-side jets, is suppressed by the beam-beam coincidence required in the Level 0 trigger (L0 Good). The Run-1a trigger (JET_END_LOW) is used to obtain a control sample of "same-side" (in rapidity) jet events. However, as this trigger has limited statistics after offline cuts, a dedicated same-side Run-1b trigger (JET_GAP_SAME) is used to obtain a much larger control sample. The same-side trigger requirements and resulting statistics are summarized in Table 4 as well.

Trigger	Level 0	Level 1	Level 2	Events
High-$\Delta\eta_c$ (`JET_GAP_MED`)	$\|z\| < 100$ L0 Good	JT(2,5,$\|\eta\| > 2$)	JT(2,25,$\|\eta\| > 2$) $\Delta\eta > 4$	77K
Same-Side (1a) (`JET_END_LOW`)	$\|z\| < 100$ L0 Good	JT(1,7,$\|\eta\| > 2$)	JT(1,30)	367K
Same-Side (1b) (`JET_GAP_SAME`)	$\|z\| < 100$ L0(1), Good	LJ(2,12,$\|\eta\| > 1.6$) LJ(1,6)LJ(2,3)	JT(2,25,$\|\eta\| > 1.6$)	165K

Table 4: Trigger requirements.

The offline cuts used in this analysis are similar to those in the first PRL and thesis and are summarized in Tables 5 and 6. The multiple interaction cut is necessary to remove events with more than one proton-antiproton interaction, which include a source of particles not associated with the triggering interaction. The opposite-side sample and same-side Run-1a sample require L0 Flag = 1, which keeps only events that are likely to have a single interaction based on the width of the time distribution of Level 0 counter hits. The Run-1b sample, which has a higher average luminosity, invokes the more stringent MI Tool = 1 requirement [38]. In addition to L0 Flag = 1, this requires only one CDC vertex, as well as a requirement on the total energy of the event, $E_{\mathrm{TOT}} < 1800$ GeV. The "Good QCD jets" cut is based on the standard "bad jet" cuts of the QCD group and requires $0.05 < \mathrm{EMF} < 0.95$, $\mathrm{CHF} < 0.4$, and $\mathrm{HOT} < 10.0$, where EMF is the EM fraction, CHF is the coarse hadronic fraction, and HOT is the ratio of the highest ET cell to the second highest ET cell. Events in which either of the leading two jets fail any cut are rejected. The other fiducial cuts are described in more detail in the thesis, and the systematic effects of the cuts will be discussed in a later section. The jet E_T, η, ϕ, leading jet E_T difference, as well as event $\not{E}_T$, $\not{E}_T/E_{T1}$, $\Delta\eta_c$, $\Delta\phi$, η_{boost}, number of jets, instantaneous luminosity and the z-vertex distributions are shown for the opposite-side trigger in Figs. 8–9 and the Run-1b same-side trigger in Figs. 10–11.

Cut	High-$\Delta\eta_c$
$N_{jets} > 2$ & $\Delta\eta_c > 0$	71718
MI Flag = 1	27999
$\lvert z\rvert < 50$ cm	26507
$\lvert\eta_1\rvert, \lvert\eta_2\rvert > 2$ $E_{T1}, E_{T2} > 30$ GeV	23387
"Good QCD jets"	22411

Table 5: Offline cuts on the high-$\Delta\eta_c$ trigger samples.

Cut	Same-side (1a)	Same-side (1b)
Same-side cuts	9328	117173
MI Cut	3652	76866
$\lvert z\rvert < 50$ cm	3646	72581
$\lvert\eta_1\rvert, \lvert\eta_2\rvert > 2$	3646	25893
$E_{T1}, E_{T2} > 30$ GeV	3646	24292
"Good QCD jets"	3467	23181

Table 6: Offline cuts on the same-side trigger samples. The "same-side cuts" for both samples includes common cuts of $N_{jets} > 2$ and $\eta_1 \cdot \eta_2 > 0$; in addition, the the Run-1a sample has jet requirements of $E_T > 30$ GeV and $|\eta| > 2$, while the Run-1b sample requires $E_T > 25$ GeV and $|\eta| > 1.6$, due to the different trigger conditions.

8 Multiplicity Measurement

In this analysis we utilize the multiplicity of electromagnetic calorimeter towers with $E_T >$ 200 MeV to measure an effective particle multiplicity distribution between jets and use this

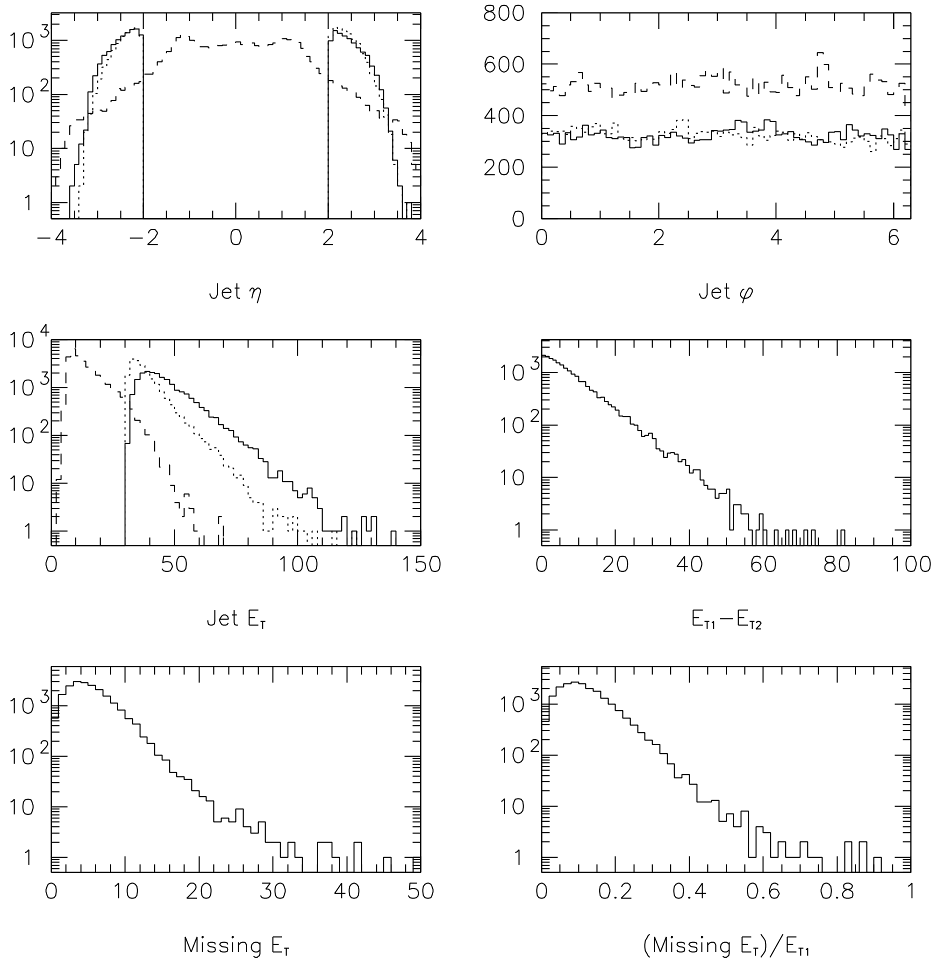

Figure 8: High-$\Delta\eta_c$ trigger: jet E_T, η, and ϕ (solid=leading jet, dotted=second jet, dashed=all other jets); E_T difference between leading jets, $\not{E}_T$, and $\not{E}_T/E_{T1}$.

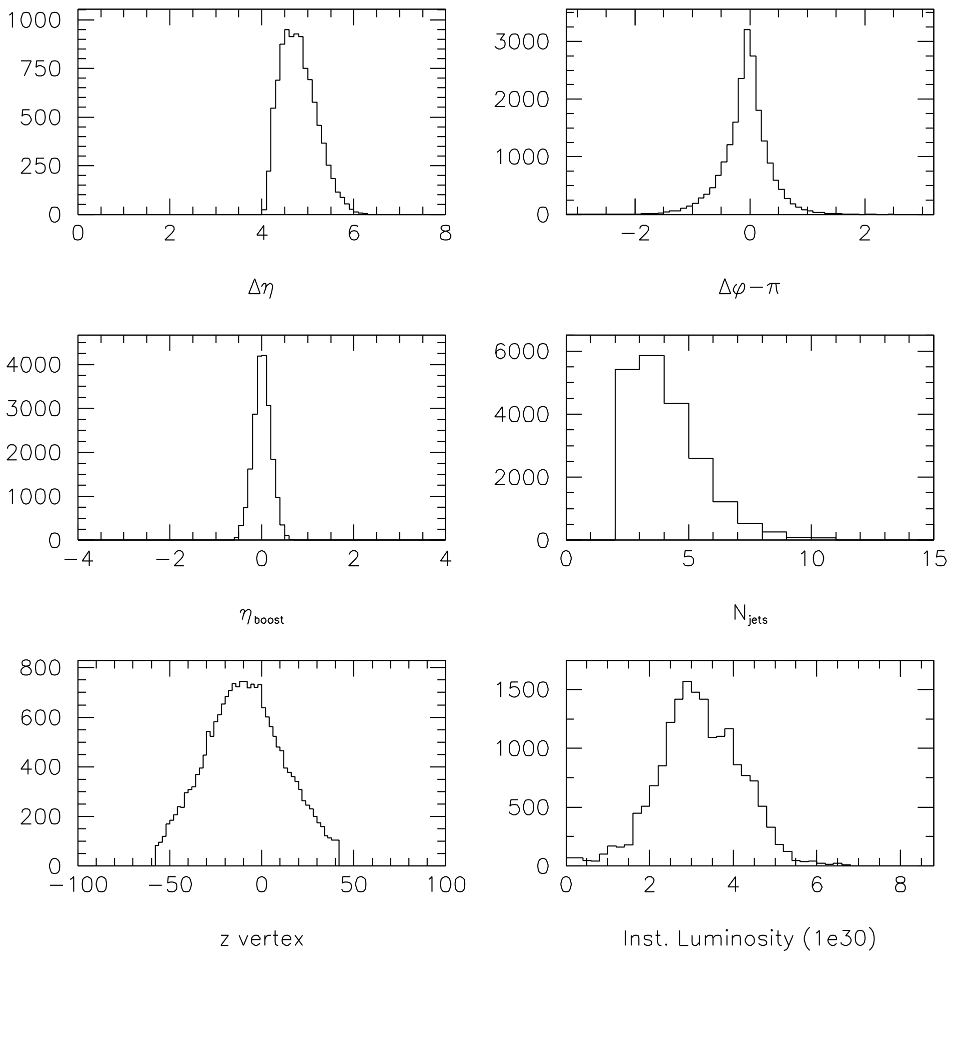

Figure 9: High-$\Delta\eta_c$trigger: $\Delta\eta$, $\Delta\phi$, η_{boost}, number of jets, instantaneous luminosity and the z-vertex distributions.

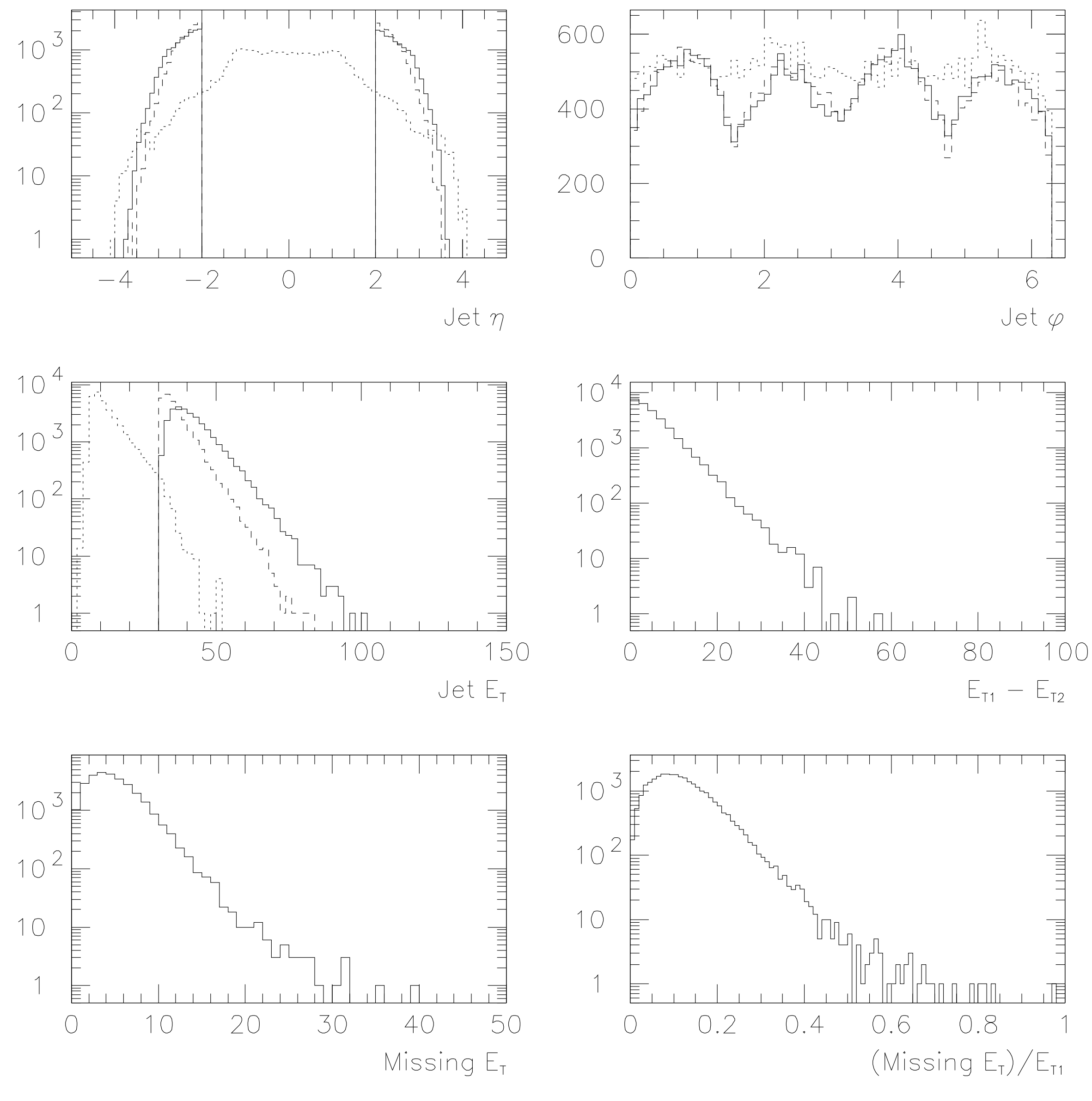

Figure 10: Same-side trigger: jet E_T, η, and ϕ (solid=leading jet, dotted=second jet, dashed=all other jets); E_T difference between leading jets, $\not{E}_T$, and $\not{E}_T/E_{T1}$.

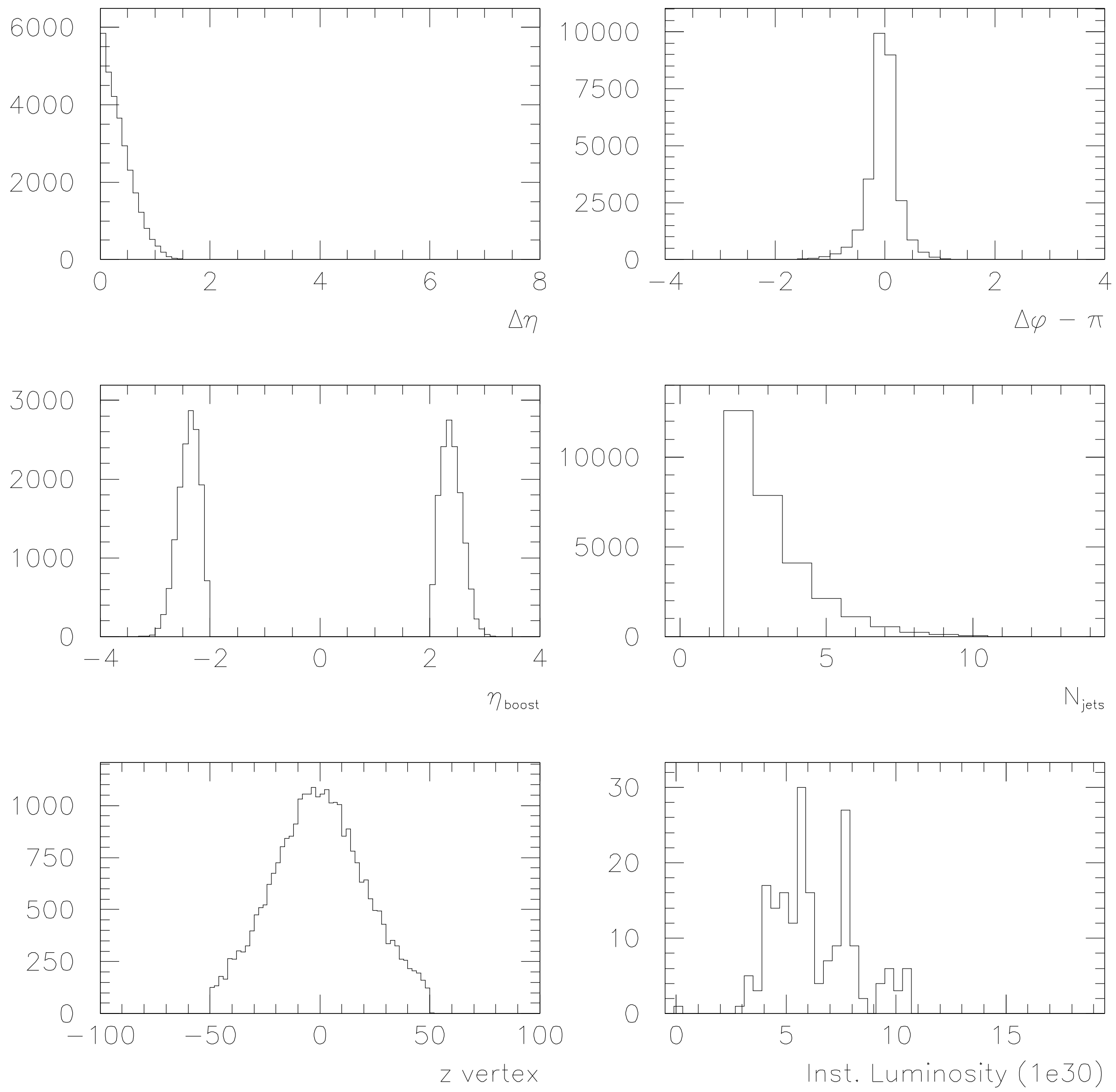

Figure 11: Same-side trigger: $\Delta\eta$, $\Delta\phi$, η_{boost}, number of jets, instantaneous luminosity and the z-vertex distributions.

to identify a signal from color-singlet exchange. The EM calorimeter is particularly useful for tagging low energy particles due to its low level of noise and reasonable tagging efficiency (see first PRL and thesis for discussion of noise, noise removal, and tagging efficiency). However, several effects can change the observed multiplicity distribution in the calorimeter. Both calorimeter noise and calorimeter shower spreading can smear the multiplicity to higher values and change the shape of the distribution. In contrast, inefficiency in detecting particles in the calorimeter can smear the multiplicity to lower values (see thesis for detailed discussion). Therefore, it is imperative to test candidate parameterizations with detector effects folded in.

The central drift chamber (CDC) is used to obtain an independent measurement of the multiplicity. The CDC has good efficiency for low energy charged particles for $|\eta| \lesssim 1.3$ and therefore can be used as a check on the calorimeter results. The tracking information is available for the entire Run-1b data sample, as well as about 70% of the Run-1a opposite side data sample. (The full Run-1a data sample includes tracking information, but this was not available on the standard RECO 10 QCD MDST's that were used for the analysis. A special MSTA project was done on the JET_GAP_MED trigger with RECO 11 to include the tracking information, but due to bad tapes and processing problems only includes a subset of about 70% of the data sample).

Figure 12 shows the impact parameter b (distance of closest approach between the track and the vertex in x and y) distribution of tracks in the final data sample. A cut of $b < 2$ cm is required for a track to be accepted.

8.1 Comparison of Opposite-Side and Same-Side Multiplicities

Figure 13(a) shows a scatter plot of the number of calorimeter towers above threshold for $|\eta| < 1.3$ versus the number of good tracks found in the CDC for the opposite-side data sample, while Fig. 13(b) shows the same quantity for the same-side data sample. There is a strong correlation between the number of tracks and towers, and the two samples are seen to be qualitatively similar. Figure 14 shows the same quantities in lego format, but zooms in on the low multiplicity region. A striking excess of events at low multiplicity is observed in the opposite-side sample (Fig. 14(a)) compared to the same-side sample (Fig. 14(b)), indicating the presence of color-singlet exchange.

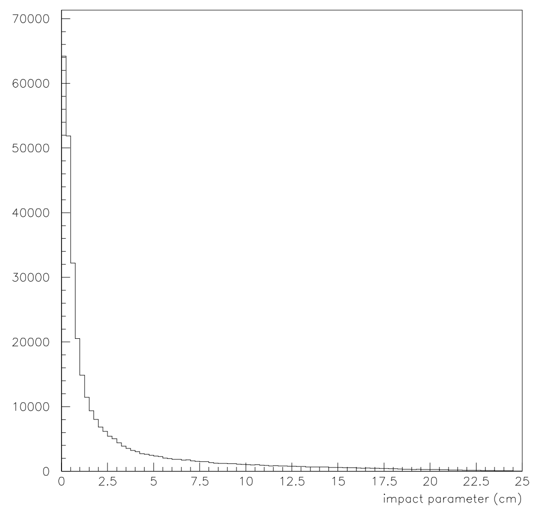

Figure 12: The impact parameter distribution for tracks from a subset of the opposite-side data sample.

9 Support for NBD-type parameterizations from Data

Although the same-side multiplicity distribution is similar to the opposite-side distribution except at low multiplicities, it does have a somewhat different mean and shape and should not be directly used as the color-exchange background. It nevertheless further supports the Monte Carlo results showing that an NBD-type parameterization gives a good description of color-exchange multiplicities. Additional data-derived support for the double NBD parameterization in color-exchange events is given by a subset of the opposite-side data sample, obtained by demanding the presence of a third jet between the leading two jets, a topology that is highly suppressed for color-singlet exchange.

We employ the tests outlined earlier on these data "control" samples to show that the NBD hypothesis is in fact valid for our data. We test the "negative-binomial-ness" of the samples (χ^2/df) and determine if there is any systematic excess at low multiplicity using the adaptive fitting method. The sections below describe the data samples used in the analysis, the experimental multiplicity measurement using the calorimeter, the support for the NBD hypothesis from the control samples, and the subsequent measurement of the excess in our

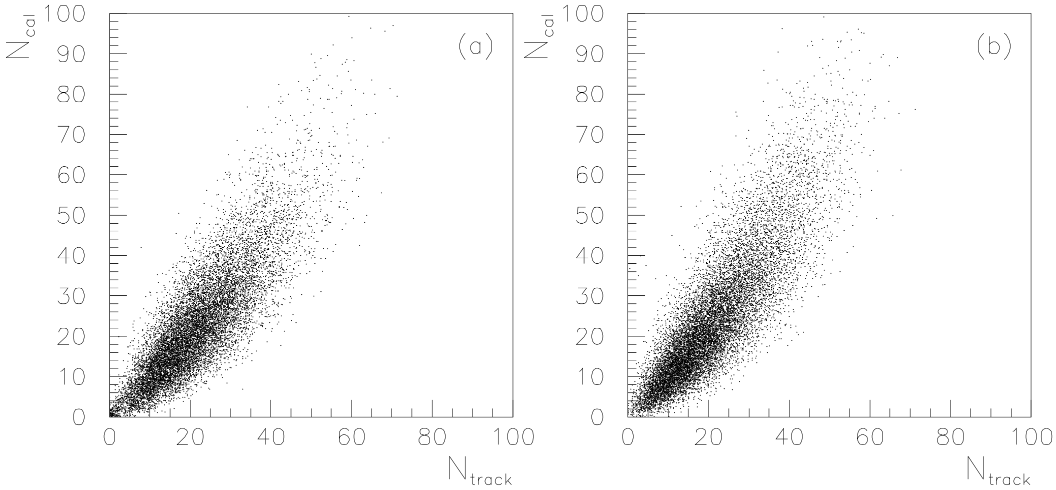

Figure 13: The calorimeter tower multiplicity distribution versus the tracking multiplicity distribution in the pseudorapidity region $|\eta| < 1.3$ for (a) the opposite-side sample and (b) the same-side sample as described in the text.

inclusive dijet (high-$\Delta\eta_c$ trigger) sample.

Same-side Multiplicity

Analysis of a "same-side" jet sample, which should give a central multiplicity distribution representative of color exchange, provides support for the NBD hypothesis in the data. Figure 15 shows that the multiplicity of EM towers in the rapidity interval $-1.0 < \eta < 1.0$ ($\Delta\eta = 2.0$) for the Run-1a sample (solid histogram) is in good agreement with the Run-1b sample (dashed histogram). Figure 16(a) and (c) show the multiplicity distributions along with the single NBD fit for the Run-1a and Run-1b samples, respectively. Figure 16(b) and (d) shows the same quantities on a log-log scale to magnify the low multiplicity region. A single NBD fit to the multiplicity distribution gives a good χ^2/df and shows no obvious excess at the low multiplicity.

Table 7 shows the χ^2/df and K-S parameter (defined in Sec. 5) along with the χ^2_5 from the adaptive fitting method. The excess from the adaptive fitting $f(n_0)$ gives identically

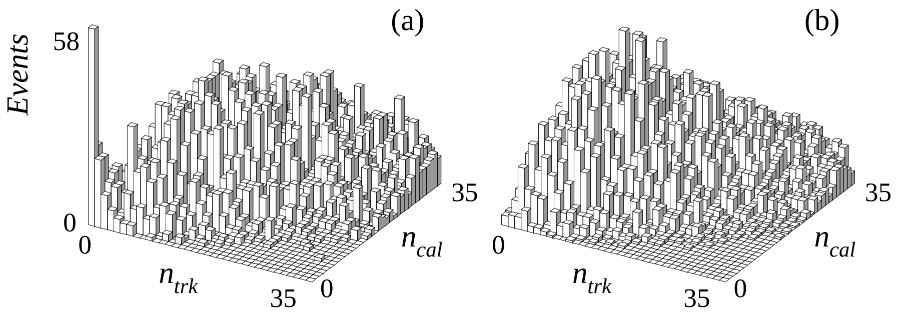

Figure 14: The calorimeter tower multiplicity distribution versus the tracking multiplicity distribution in the pseudorapidity region $|\eta| < 1.3$ for (a) the opposite-side sample and (b) the same-side sample as described in the text.

zero—since $\chi^2_5 < 2$ for $n_0 = 0$, there is by definition no excess. Forcing the fit to start from $n_0 = 1$ gives the $f(1)$ column, which shows a small statistically insignificant excess for the low statistics Run-1a sample and no significant excess for the Run-1b sample. The superior statistics of the Run-1b sample allow for a double NBD fit, which yields virtually identical results to the single NBD fit, with a slightly smaller K-S parameter indicating a somewhat better fit. The Run-1b same-side sample, with statistics comparable to the opposite-side sample clearly demonstrates that no significant low multiplicity excess is expected from color exchange or from detector effects generating an artificial excess.

Sample	NBD	χ^2/df	C.L.	K-S stat.	χ^2_5/df	C.L.	$f(n_0)$	$f(1)$ (%)
1a	Single	1.06	34%	3.74	1.9	9.5%	0	0.29 ± 0.15
1b	Single	1.00	48%	3.92	0.7	68%	0	-0.038 ± 0.039
1b	Double	0.92	68%	1.24	0.3	90%	0	-0.038 ± 0.039

Table 7: NBD Fits to the same-side multiplicity distributions for $\Delta\eta = 2$. The multiplicity distributions are fit using ($n_0 = 0$) since $\chi^2_5 < 2$ for each fit. Shown is χ^2/df and associated confidence level (C.L.), the Kolmogorov-Smirnov statistic (K-S stat.), χ^2_5 and associated C.L., the fractional excess above the fit for $n < n_0$ ($f(n_0)$), and the fractional excess $f(1)$ (in %) when the fit is forced to start at $n_0 = 1$.

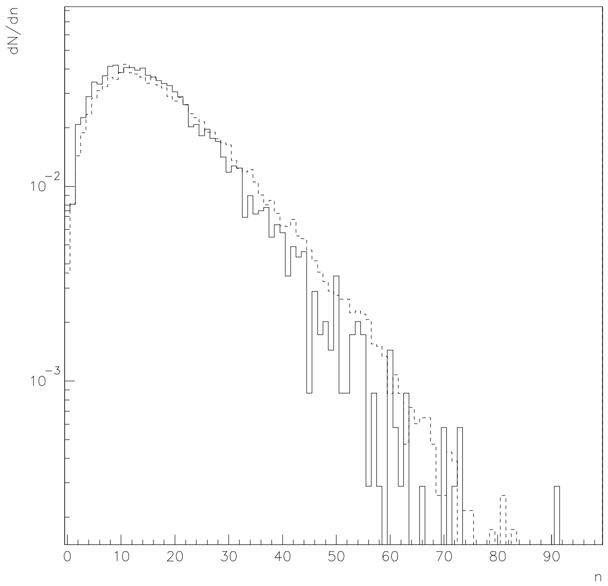

Figure 15: The calorimeter tagged-particle multiplicity distributions for the Run-1a (solid histogram) and Run-1b (dashed histogram) same side samples in the region $\Delta\eta < 2$.

Three-jet Multiplicity

Further support for the NBD is shown in a sample of color-exchange enhanced data that are obtained by demanding the presence of a third jet between the leading two jets—a topology which would be highly suppressed for color singlet exchange due to the "hard" radiation between the jets. Figure 17 shows the multiplicity of EM towers for the subset of opposite-side events with an additional jet in the $\Delta\eta_c$ region between the leading two jets and the resulting double NBD fits. The multiplicity is plotted for the full $\Delta\eta_c$ region except that a region around the third jet is excluded to avoid biases from the multiplicity of this jet. Figure 17(a-b) excludes a region of radius 0.7 about the third jet axis, while Fig. 17(c-d) excludes a region of radius 1.0.

Table 8 shows the χ^2/df and K-S parameter along with the χ^2_5 from the adaptive fitting method. The double NBD fits are preferred to the single NBD fits and give a good χ^2 and little significant excess at low multiplicity. The excess $f(1)$ is given starting the fit at $n_0 = 1$

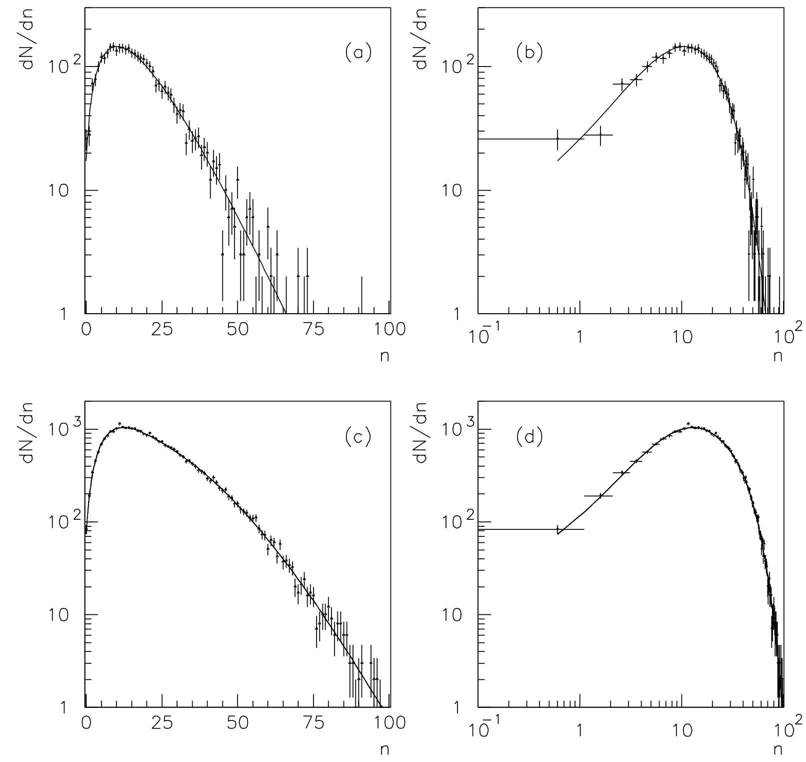

Figure 16: The calorimeter tagged-particle multiplicity distributions ($|\eta| < 1$) and single NBD fits to the multiplicity for (a) the Run-1a same-side sample (b) log-log version (c) the Run-1b same-side sample (c) log-log version.

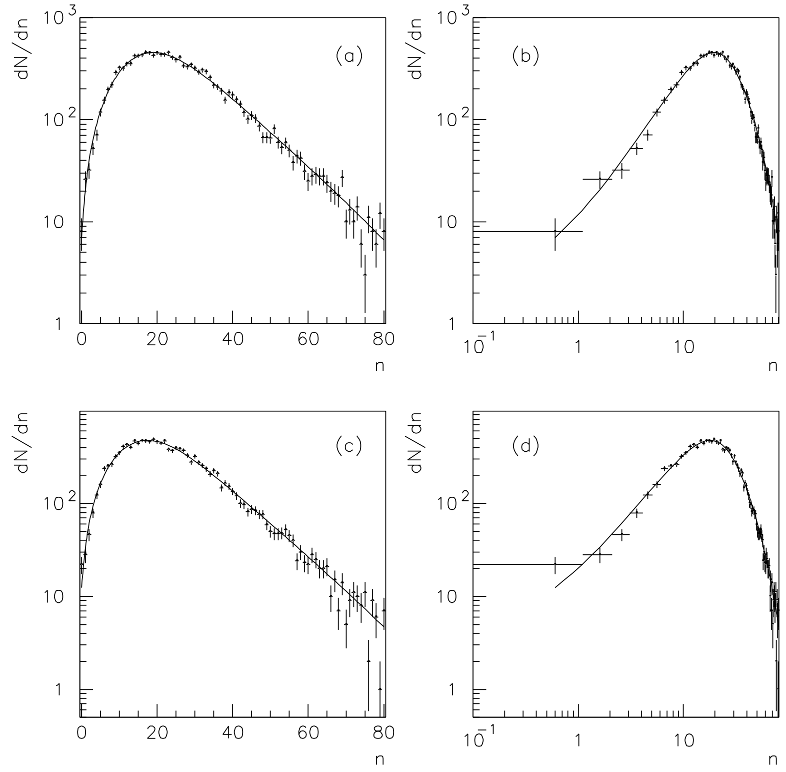

Figure 17: The calorimeter tagged-particle multiplicity distributions for opposite-side events that have a third jet in the region between the leading two jets (a) excluding a region of $R = 0.7$ around the third jet (b) log-log version (c) excluding a region of $R = 1.0$ around the third jet (d) log-log version. The double NBD fits to the data samples are also shown.

and extrapolating to $n = 0$, since for these samples this gives the largest (most conservative) value for the excess. Thus these "tagged" color-exchange events (a small amount of color-singlet contamination is expected) give further support for the NBD hypothesis, and again show that detector effects do not create any significant low multiplicity excess.

The NBD Hypothesis

The same-side samples indicate that a single NBD gives an excellent fit to the color-exchange data over the entire range of multiplicity. The opposite-side color-exchange enhanced sample also have good fits and little excess at low multiplicity, but are better described by a double

Cone	NBD	χ^2/df	C.L.	K-S stat.	χ_5^2/df	C.L.	$f(1)$
0.7	Single	1.63	0.2%	36.76	3.6	0.1%	0.017 ± 0.021
0.7	Double	1.23	5.2%	4.62	2.1	5.3%	0.008 ± 0.021
1.0	Single	1.62	$< 10^{-4}$	28.16	1.7	13%	0.094 ± 0.034
1.0	Double	1.39	0.5%	3.56	2.1	5.6%	0.079 ± 0.034

Table 8: NBD Fits to the 3-jet multiplicity distributions for $\Delta\eta = 2$. The multiplicity distributions are fit using various starting points (n_0) for each fit. Shown for $n_0 = 1$ is χ^2/df and associated confidence level (C.L.), the Kolmogorov-Smirnov statistic (K-S stat.), χ_5^2 and associated C.L., and the fractional excess $f(1)$ (in %) when the fit is forced to start at $n_0 = 1$.

NBD. As discussed previously, the PYTHIA MC study indicates that the double NBD fits opposite-side distributions better than the single NBD. In this analysis we fit a double NBD to the opposite-side data, and show that a single NBD is excluded due to shape differences.

10 Measurement of the Excess in the Opposite-Side Multiplicity Distribution

The low multiplicity excess observed in Fig. 14(a) is measured using the following procedure (i.e. the adaptive fitting method described in Sec. 5). First a double NBD is fit to the entire opposite-side calorimeter multiplicity distribution using the maximum likelihood method. The parameters are allowed to vary except for the overall normalization, which is set to the number of events in the fitted region, and the relative normalization, which is determined by minimizing the modified Kolmogorov-Smirnov (K-S) statistic defined as the sum of the squared differences between the cumulative distributions of the data and the fits (see Sec. 5). Next, the starting bin (n_0) for the fit is incremented by one and the remaining bins refitted until the χ^2/df in the first five bins of the fit is less than 2.0 (i.e. C.L. $>$ 93%). The fit is then extrapolated to zero multiplicity in order to determine the excess above the color-exchange background for $n < n_0$.

Figure 18(a-b) shows the calorimeter tagged-particle multiplicity between the two highest E_T jets for the whole opposite-side sample. Also shown is the double NBD fit and its extrapolation to zero multiplicity. In contrast with the color-exchange Monte Carlo and background data samples, the opposite-side sample has a statistically significant excess at low multiplicity.

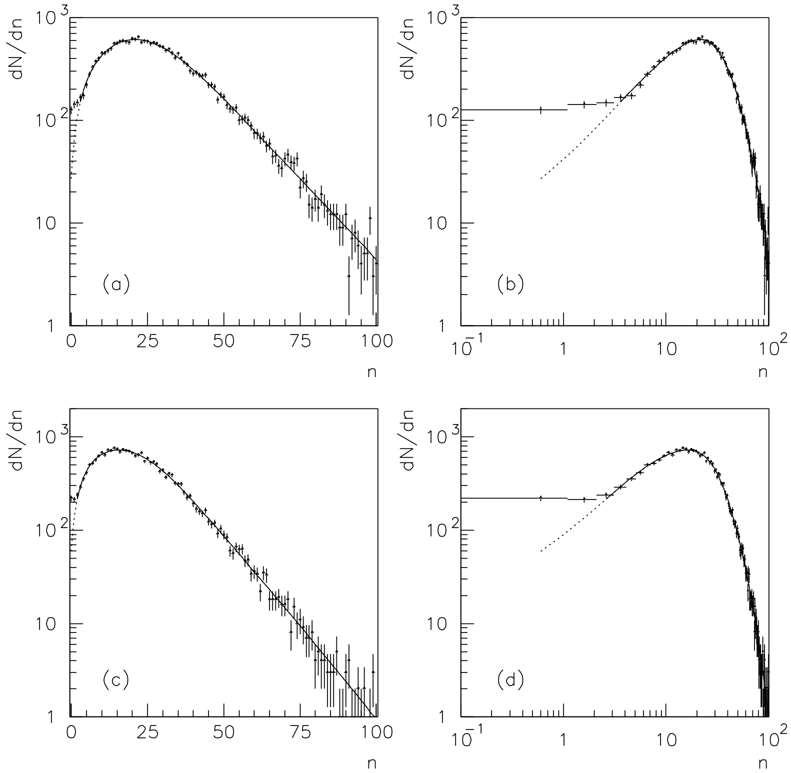

Figure 18: The calorimeter tagged-particle multiplicity distributions for the full opposite-side sample ($\Delta\eta_c > 2.6$). Figures (a) and (b) (log-log) show the multiplicity distribution in the region between the edges of the jet cones. Figures (c) and (d) (log-log) show the multiplicity distribution in the region $|\eta| < 1$. The solid lines represent the double NBD fits, while the dotted line shows the extrapolation of each fit to $n = 0$.

Figure 18(c-d) shows the tagged-particle multiplicity for the same events but in a smaller central pseudorapidity region ($|\eta| < 1$) corresponding to the central calorimeter. This has the advantage of significantly reducing any experimental out-of-cone effects that could artificially lower the excess by smearing a low multiplicity signal to higher multiplicity. Out-of-cone effects include particles associated with the jet that are emitted outside of a fixed jet cone, and particles within the cone that deposit energy outside of the cone due to calorimeter shower broadening. As shown in the figure, the distribution is shifted to lower multiplicities, but its shape (excluding low multiplicity bins) also is fit well by a double NBD, and a clear excess is again present at low multiplicity.

Table 9 shows the results of double NBD fits to the two distributions in Fig. 18 as a function of n_0, the starting point for the fits. The quality-of-fit, number of events above the fits for $n < n_0$, and the fractional integrated excess $f(n_0)$ are shown as a function of n_0. For both η regions, fits with starting points of $n_0 < 2$ are excluded. An excess of $225 \pm 20\,(237 \pm 21)$ events is observed for Figs. 18(a) and (c), respectively.

The fractional excess f_S is defined as the average excess above the double NBD fit for starting points of n_0 and $n_0 + 1$, divided by the total number of events. This definition reduces the uncertainty due to the choice of fit starting point. A low multiplicity fractional excess of $f_S = 1.07\,(1.14) \times 10^{-2}$ is measured for the two regions, respectively. Table 10 shows the effect of varying the relative normalization of the two NBD's used in the fits. The fits that give the smallest K-S parameter have been used as the default fits shown in Figure 18 and to determine the excess given above.

Multiplicity between jet cones							
n_0	χ^2/df	C.L.	K-S stat.	χ_5^2/df	C.L.	$N(n_0)$	$f(n_0)$ (%)
0	2.12	$< 10^{-6}$	9.76	25.3	$< 10^{-6}$	—	—
1	1.36	0.4%	2.31	11.5	$< 10^{-6}$	92.4	0.41
2	1.00	48%	0.58	3.8	0.1%	173	0.77
3	0.90	78%	0.42	1.3	26%	225	1.00
4	0.88	82%	0.50	0.7	64%	256	1.14
f_S						241 ± 22	1.07 ± 0.10
Multiplicity in $\Delta\eta = 2$							
n_0	χ^2/df	C.L.	K-S stat.	χ_5^2/df	C.L.	$N(n_0)$	$f(n_0)$ (%)
0	2.45	$< 10^{-6}$	9.84	25.5	$< 10^{-6}$	—	—
1	1.24	4.8%	1.38	5.2	$< 10^{-3}$	150	0.67
2	0.99	52%	0.60	0.9	51%	237	1.06
3	0.97	57%	0.60	0.4	83%	274	1.22
f_S						255 ± 23	1.14 ± 0.10

Table 9: Double NBD fits to the multiplicity distributions between jets for events with $\Delta\eta_c > 2.6$. The multiplicity distribution in two detector regions (in a $\Delta\eta_c$ region between the jets and a fixed region of $\Delta\eta = 2$) are fit using various starting points (n_0) for each fit. Shown is χ^2/df and associated confidence level (C.L.), the Kolmogorov-Smirnov statistic (K-S stat.), χ_5^2 and associated C.L., the excess number of events above fit for $n < n_0$ ($N(n_0)$), and the integrated fractional excess $f(n_0)$ (in %) as a function of fit starting point n_0. The row denoted f_S gives the average of the excess for n_0 and $n_0 + 1$ for which $\chi_5^2(n_0)/df < 2.0$.

Region	Ratio	0.55	0.65	0.75	0.80	0.85	0.90	0.95	1.00
$\Delta\eta_c > 2.6$	K-S	0.66	0.53	0.43	0.42	0.48	0.95	5.53	14.45
	f_S	0.93	0.98	1.04	1.07	1.12	1.19	1.29	1.54
$\Delta\eta = 2$	K-S	0.90	0.78	0.67	0.63	0.60	0.65	2.16	5.79
	f_S	0.92	0.98	1.05	1.09	1.14	1.21	1.55	2.00

Table 10: The effect of varying the relative normalization of the two NBD's used in the fits. The K-S parameter value (For fits with starting point of n_0) is shown along with the measured excess f_S. Ratios with the smallest value of the K-S parameter (0.80 and 0.85, respectively) are used as the default fits for the two regions.

10.1 Systematic Error in Fit Parameterization

The systematic error from fitting the background multiplicity distribution is determined by varying the fit parameters (to produce a 1σ change in χ^2) and redetermining the excess. The error is taken as the difference between f_S and the largest and smallest value for the excess found by varying the fit parameters. Table 11 shows the results. The error is conservatively taken as plus/minus the largest difference in the excess. Varying the endpoint of the fits (i.e. last multiplicity bin fit) results in less than a 1% change in the excess.

An additional error from the uncertainty in the relative normalization of the two NBD's (see Table 10) is determined by varying the the ratio of the two NBD's by $\pm 5\%$ and taking the maximum difference. From Table 10, this error is $\pm 5.7\%$. The total error for the two regions is $\pm 10.6\%$ and $\pm 9.7\%$, respectively.

We note that this systematic error does not include possible effects from using a parameterization other that a double NBD. Although we have not exhaustively spanned the space of all possible parameterizations, we have shown that the double NBD fits both data and Monte Carlo color-exchange samples well, which is sufficient for this measurement.

η Region	f_S	Min	Max	Difference		% Error
$\Delta\eta_c > 2.6$	1.073	0.946	1.135	-0.082	+0.095	± 8.9
$\Delta\eta = 2$	1.140	1.067	1.228	-0.073	+0.088	± 7.8

Table 11: Error due to the double NBD fit parameters on the measured excess.

10.2 Comparison with Single NBD fit

The low multiplicity excess has previously been measured using single NBD fits to the multiplicity between jets [39]. Although both the single and double NBD give reasonable fits

(χ^2/df = 1.1 and 0.9, respectively) to the opposite-side multiplicity distributions, K-S shape tests show systematic differences between the single NBD fits and the data. Figure 19(a) shows the double NBD fit to the multiplicity between the jet edges for the opposite-side sample on a linear scale. Figure 19(b) shows the single NBD fits to the same data, which again gives a reasonable fit with a clear low-multiplicity excess, but unlike the double NBD shows a systematic relative skewness between the data and the fit. This difference is evident in the χ^2 and K-S value as discussed below.

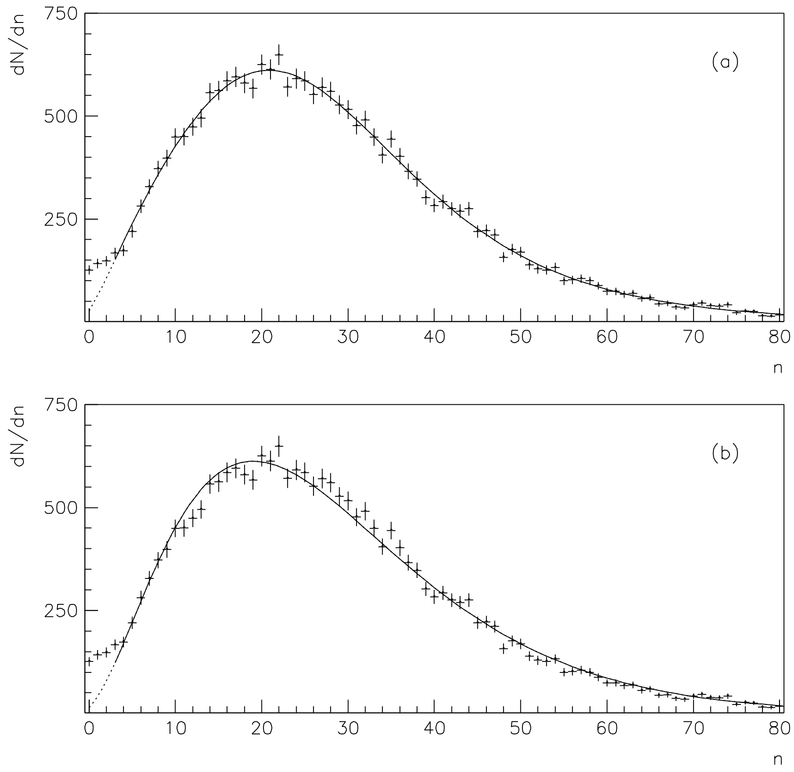

Figure 19: The calorimeter tagged-particle multiplicity distributions between the jet edges for all opposite-side jet events with $\Delta\eta_c > 2.6$. The solid lines represents the (a) double NBD fit and (b) single NBD fit while the dotted line shows the extrapolation of each fit to $n = 0$.

Table 12 shows the results of single NBD fits to the two multiplicity distributions. Comparing with Table 9 (i.e. the double NBD fits) shows that:

- The overall χ^2/df is larger (> 1.0), but doesn't exclude all fits.
- The K-S statistic is about 10 times larger, indicating large systematic differences between the fit and the data as opposed to the double NBD fits. The double NBD is significantly favored over the single NBD (discussed below).
- The measured excess is significantly larger, $1.5\,(2.0) \times 10^{-2}$ for the two η regions, indicating a systematic difference in the two fit parameterizations.

To quantify the difference in the quality of the single and double NBD fits, we have generated a Monte Carlo sample of 500 pseudo-multiplicity distributions using the measured multiplicity distribution as the underlying probability distribution (i.e. Fig. 18(a-b)). (This is akin to a "bootstrap" method.) We then fit each pseudo-multiplicity distribution with both a single and double NBD and calculate the K-S value for each. Figure 20 shows the measured K-S value for both fits. All of the double NBD fits have a lower K-S value than any of the single NBD fits. Thus no single NBD fit gives a K-S value (i.e. goodness of fit) as small as any of the double NBD fits. The probability for a single NBD fit to give a K-S value as small as any value from a double NBD fit is less than 0.01% as determined from fitting each K-S distribution to a Gaussian. Thus, the double NBD is highly favored (by a factor of $> 10^5$ in this comparison) over the single NBD.

As an additional test, we calculate the likelihood values for each fit and compare them by taking the ratio. We assume that the number of events in each bin is described by a Poisson distribution and that the fits give the expected value in each bin. Thus, the probability for the observed value in each bin can be calculated using the Poisson distribution and the expected number of events. The "likelihood" probability for the data observed given the fit hypothesis is defined as the product of these probabilities for all bins that are fit. We obtain a likelihood ratio of 10^{12} for the double NBD over the single NBD. Thus the double NBD has a much higher likelihood (probability) to describe the data and is highly favored over the single NBD.

We note that this is not a proof that the distribution has the underlying form of a double NBD (i.e. no fit can be "proved"), only that compared to a single NBD the double NBD gives a significantly smaller systematic difference between the fit and the data. If the single NBD were a good parameterization of the measured multiplicity distribution, adding a few additional parameters should not affect the goodness of fit significantly. Of

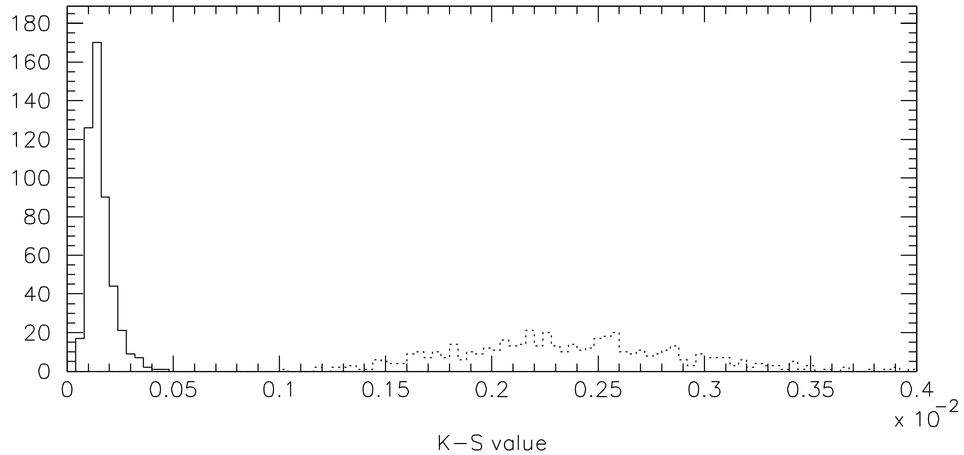

Figure 20: The K-S values for double NBD (solid) and single NBD (dotted) fits to the pseudo-sample.

course, further increasing the number of parameters (i.e. approaching the number of d.o.f) would approach a perfect goodness of fit which is statistically unlikely. Thus choosing a parameterization is not well-defined analytically (from first principles) and is a balance of quantitative supporting evidence (goodness of fit measures), and a good eye (i.e. common sense). We choose the double NBD to parameterize the multiplicity from color exchange since it satisfies these criteria better than any other reasonable function we have attempted to fit (but we are continuing to search for alternative methods/parameterizations for this measurement).

10.3 Particle Tagging Effects

The excess has been found to be relatively insensitive to the particle tagging method (within errors). We compare the excess using several different particle tagging methods and conservatively assign a systematic error to the method.

Effect of Tower Threshold

The calorimeter EM tower threshold has been varied in order to determine if there is a systematic effect due to the tower particle tagging method. Figure 21 shows the effect of

Multiplicity between jet cones							
n_0	χ^2/df	C.L.	K-S stat.	χ_5^2/df	C.L.	$N(n_0)$	$f(n_0)$
0	3.26	$< 10^{-6}$	74.61	31.7	$< 10^{-6}$	—	—
1	1.53	$< .01\%$	39.19	7.1	$< 10^{-6}$	205	0.92
2	1.24	3.6%	21.70	2.4	2.5%	281	1.25
3	1.11	19%	14.45	0.6	74%	339	1.51
4	1.11	19%	11.33	0.6	71%	352	1.57
f_S						345 ± 26	1.54 ± 0.11
Multiplicity in $\Delta\eta = 2$							
n_0	χ^2/df	C.L.	K-S stat.	χ_5^2/df	C.L.	$N(n_0)$	$f(n_0)$
0	3.64	$< 10^{-6}$	59.01	31.8	$< 10^{-6}$	—	—
1	1.94	$< 10^{-6}$	22.64	10.2	$< 10^{-6}$	171	0.77
2	1.39	0.5%	11.53	3.6	0.1%	286	1.28
3	1.23	5.8%	7.63	2.0	6.4%	361	1.61
4	1.17	12.3%	5.79	1.3	26%	421	1.89
5	1.14	16.7%	4.75	1.0	46%	474	2.12
f_S						448 ± 34	2.00 ± 0.15

Table 12: Single NBD fits to the multiplicity distributions between jets for events with $\Delta\eta_c > 2.6$. The multiplicity distribution in two detector regions (in a $\Delta\eta_c$ region between the jets and a fixed region of $\Delta\eta = 2$) are fit using various starting points (n_0)for each fit. Shown is χ^2/df and associated confidence level (C.L.), the Kolmogorov-Smirnov statistic (K-S stat.), χ_5^2 and associated C.L., the excess number of events above fit for $n < n_0$ ($N(n_0)$), and the integrated fractional excess $f(n_0)$ (in %) as a function of fit starting point n_0. The row denoted f_S gives the average of the excess for n_0 and $n_0 + 1$ for which $\chi_5^2(n_0)/df < 2.0$.

increasing the 200 MeV threshold to 250 MeV and 300 MeV. Increasing the threshold lowers the particle detection efficiency and thus reduces the multiplicity as shown in Fig 21(a). Figure 21(b) shows the double NBD fit for the 250 MeV threshold which gives an excess of 1.09%. Fig. 21(c) shows the double NBD fit for the 300 MeV threshold. Although the 300 MeV threshold still gives a significant excess, it is slightly lower due to the larger uncertainty in the fit starting point caused by the lower mean of the distribution.

Effect of Clustered Towers

Calorimeter shower spreading results in smearing the multiplicity to higher values because a single particle can produce multiple EM towers. In order to test the effect of shower spreading, we measure the multiplicity of calorimeter "clusters" found using a simple cone

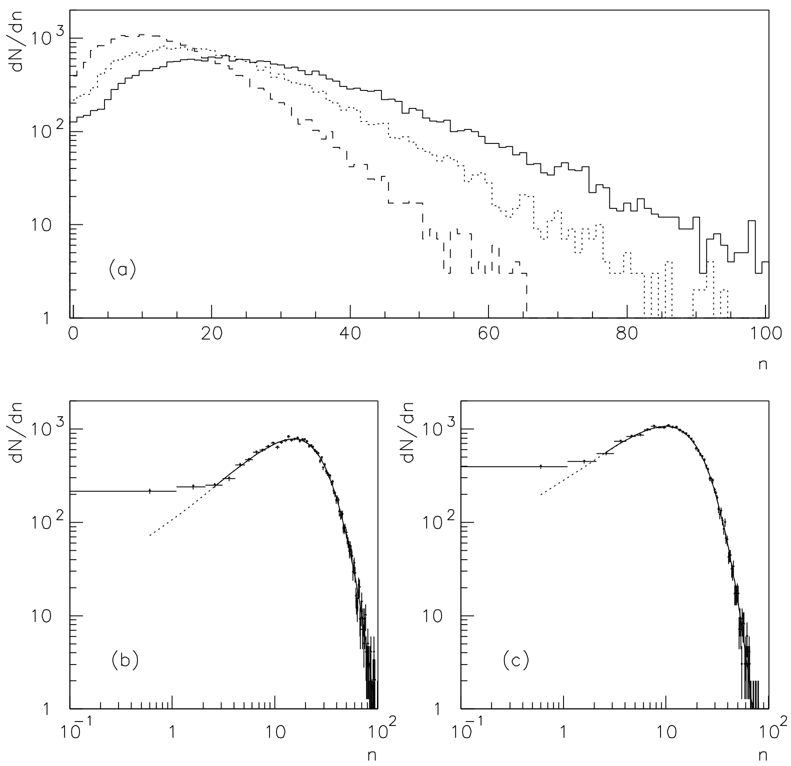

Figure 21: The calorimeter tagged-particle multiplicity distributions as a function of calorimeter shower threshold, for all opposite-side jet events with $\Delta\eta_c > 2.6$. (a) compares three thresholds 200 MeV (solid), 250 MeV (dotted), and 300 MeV (dashed). (b) and (c) show the multiplicity distribution for 250 MeV and 300 MeV, respectively. The solid lines represent the double NBD fits, while the dotted line shows the extrapolation to $n = 0$.

clustering algorithm. Figure 22 shows the multiplicity distribution obtained using a cone of $R = 0.15$. The distribution is consistent with a double NBD, but the parameters of the fit change significantly compared to Fig. 18(a-b). The excess obtained from clustering in cones of $R = 0.15$ and 0.29 (equivalent to 3×3 and 5×5 block of calorimeter towers, respectively) is 1.07% and 1.23%.

Effect of using Tracking Multiplicity

We have also measured the excess using the track multiplicity in the CDC (with an impact parameter cut of $b < 2\,\mathrm{cm}$). Figure 23 shows the multiplicity distribution and double NBD fit. The shape is different from Fig 18(c-d), but the excess of 1.25% is consistent within

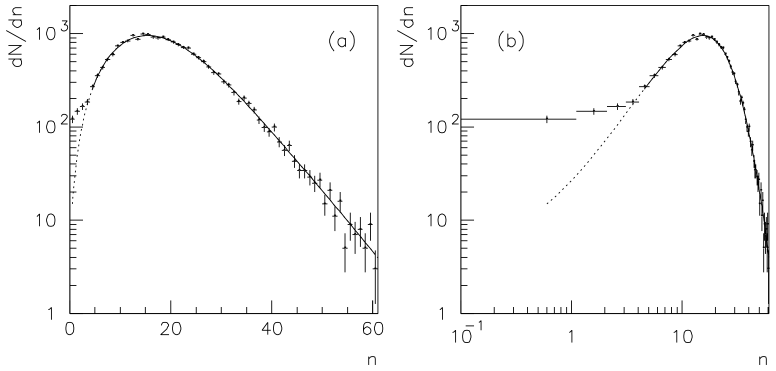

Figure 22: The clustered tower multiplicity distribution for all opposite-side jet events with $\Delta\eta_c > 2.6$ for the region between the jets. Figure (b) shows log-log plot of (a). The solid lines represent the double NBD fits, while the dotted line shows the extrapolation to $n = 0$.

errors. Making an additional requirement of $|\eta| < 1.3$ and 1.0 on the tracks, gives an excess of 1.22% and 1.11%, respectively. The excess was found also to be relatively insensitive to cuts on the impact parameter or distance between the track and vertex cuts.

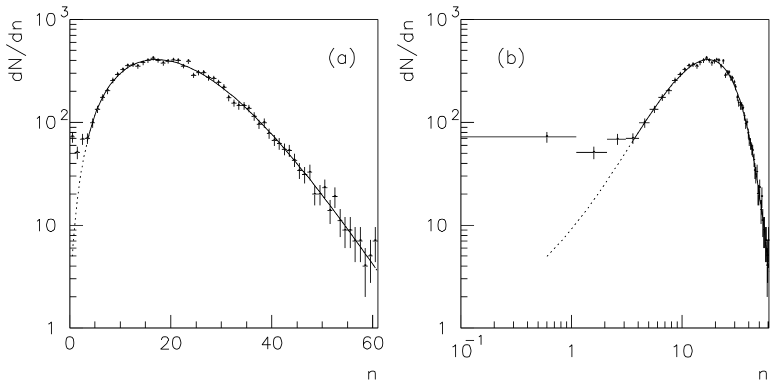

Figure 23: The tracking multiplicity (CDC) distribution for all opposite-side jet events with $\Delta\eta_c > 2.6$. Figure (b) shows log-log plot of (a). The solid lines represent the double NBD fits, while the dotted line shows the extrapolation to $n = 0$.

Systematic Error from Tagging Method

As demonstrated above, the measured fractional excess is relatively insensitive to the details of the particle tagging method. Varying the calorimeter tower E_T threshold and refitting the multiplicity gives different parameters but a consistent excess. Clustering neighboring calorimeter towers using a cone algorithm to define each cluster as a particle gives an excess that is consistent with the standard method, but about 0–15% larger. Using charged charged tracks instead of calorimeter towers to calculate the excess also gives a slightly larger result ranging from 3–17%. We thus assign a +15% systematic error due to the choice of tagging method.

10.4 Systematic Error from Cuts

We have investigated the effects of our offline cuts on the measured excess. We vary the cuts within a reasonable range of values and redo the analysis (fitting and measuring the excess) in order to determine the systematic error. To be conservative the error is taken as plus or minus the maximum difference between f_S and the redetermined excess. The largest error from either region is used as the systematic for each effect. We note that for the cuts varied below, the multiplicity distributions do not change discernibly as the effects are on the order of 5%.

"Good" Jet Requirement

To determine if there is a bias from the good jet requirement on the leading jets, we redetermine the excess using: (1) no requirement, (2) good jet requirement on all jets, and (3) the standard QCD_FLAG (which uses nearest neighbor algorithm on all jets to determine if the event is bad). Table 13 shows the effect of good jet cuts on the measured excess. The error is taken as ±4.4%.

η Region	f_S	No cut	All	Stand.	Max. diff.	% Error
$\Delta\eta_c > 2.6$	1.073	1.052	1.120	1.068	0.047	4.4
$\Delta\eta = 2$	1.140	1.129	1.186	1.113	0.046	4.0

Table 13: Effect of good jet cuts on the measured excess.

Trigger η

The trigger cuts η of the jets are reapplied at the offline level. We determine the effect of the η cut by comparing the excess for no cut and for $|\eta| > 2.2$. Table 14 shows the results. The systematic error is taken as ±1.4%.

η Region	f_S	no cut	$\lvert\eta\rvert > 2.2$	Max. diff.	% Error
$\Delta\eta_c > 2.6$	1.073	1.071	1.082	0.009	0.8
$\Delta\eta = 2$	1.140	1.156	1.145	0.016	1.4

Table 14: Effect of jet trigger η cuts on the measured excess.

Energy Scale

The jet energy scale correction is varied $\pm 1\sigma$ in order to determine its effect as shown in Table 15. The systematic error is taken as $\pm 1.4\%$.

η Region	f_S	low	high	max. diff.	% Error
$\Delta\eta_c > 2.6$	1.073	1.073	1.083	0.010	0.9
$\Delta\eta = 2$	1.140	1.130	1.156	0.016	1.4

Table 15: Effect of varying the jet energy scale correction on the measured excess.

Multiple Interactions

In this analysis, we use the multiple interaction flag to identify events with single interactions. The flag is estimated to have 5% contamination from multiple interaction events [38], however, this does not necessarily correspond to a 5% effect in f_S. Varying the L0 multiple interaction flag cut changes the shape of the multiplicity distributions (and f_S), most likely due to a dependence of efficiency and contamination on event multiplicity.

We use a variation of the multiple interaction tool [38] to determine the systematic error on f_S from the uncertainty in tagging single interactions. We vary the multiple interaction flag cut (as in the standard tool) but also restrict events to contain only one reconstructed vertex. Table 16 shows the excess obtained by requiring a single vertex and varying the flag cut.

The range of flag cut (spanning a rather stringent cut to no cut) is very likely to contain the actual value of f_S, and the uncertainty in the excess is expected to be smaller than shown here. We therefore take half the maximum difference of the values from f_S as a conservative systematic error ($^{+14.2}_{-4.5}\%$)

11 Measured Excess

Table 17 shows the measured value of f_S including all systematic errors discussed above.

η Region	f_S	Flag=1	Flag=1,2	No Flag cut	Diff	% Error
$\Delta\eta_c > 2.6$	1.073	1.399	1.176	1.008	$^{+0.326}_{-0.064}$	$^{+14.2}_{-3.0}\%$
$\Delta\eta = 2$	1.140	1.353	1.111	1.038	$^{+0.213}_{-0.102}$	$^{+9.4}_{-4.5}\%$

Table 16: Effect of varying the single interaction requirement (multiple interaction flag plus a single vertex requirement) on the measured excess.

η Region	f_S (in %)
$\Delta\eta_c > 2.6$	$1.07 \pm 0.10(\text{stat})^{+0.25}_{-0.13}(\text{syst})$
$\Delta\eta = 2$	$1.14 \pm 0.10(\text{stat})^{+0.27}_{-0.13}(\text{syst})$

Table 17: Measured excess f_S.

Although the low-multiplicity excess is unmistakable in the opposite-side sample, theoretical interpretation of its value is complicated by uncertainties in the survival probability. In contrast with our previous measurement which used the number of events with zero multiplicity to place an upper limit on the rapidity gap fraction $((\sigma_{\text{singlet}}/\sigma) \times S)$ [1], the measurement of f_S could include some portion of the color-singlet events with low multiplicity spectator interactions. Nevertheless, the value of f_S is consistent with the 1–3% expected for strongly-interacting color-singlet exchange, and can be used to obtain a lower limit on the fraction of dijet events with color-singlet exchange and exclude purely electroweak color-singlet exchange.

12 Lower Limit

The smaller measured value of the excess is used to determine a lower limit on the fraction of events from color-singlet exchange. Combining the statistical and systematic errors in quadrature, gives a lower limit of

$$\sigma_{\text{singlet}}/\sigma_{\text{dijet}} > 0.80\%$$

at the 95% confidence level, independent of survival probability. This is to be compared with the rough estimates of 10% for Pomeron exchange and 0.1% for electroweak exchange discussed earlier. The lower limit is inconsistent with purely electroweak color-singlet exchange.

13 Exclusion of Pure EW Exchange

The observed fraction of events above the expectation for quark/gluon exchange can not be explained by electroweak color-singlet exchange plus color-exchange background alone. The fraction of dijet events from electroweak exchange has been calculated to be $\sigma_{\rm EW}/\sigma_{\rm dijet} \approx 7\times10^{-4}$ at leading order [10]. A PYTHIA Monte Carlo study using simulated DØ acceptance and efficiency for jets gives a value of $\sigma_{\rm EW}/\sigma_{\rm dijet} \approx 9\times10^{-4}$ which is comparable but also includes higher-order radiative effects (Sec. 2). The measured value for the excess in Table 17 is a factor of 10 greater than $\sigma_{\rm EW}/\sigma_{\rm dijet}$.

To determine the the probability that electroweak color-singlet exchange and the color-exchange background can fluctuate up to the observed excess we do a counting experiment. First, we determine the expected number of events at low multiplicity from the color-exchange background (using the extrapolation of the double NBD fit), and electroweak exchange. We use the maximum observable value for electroweak exchange which assumes a survival probability of 100%, i.e. all events with electroweak exchange survive spectator interactions and are observed with zero multiplicity. Next we determine the error on the expected number of events from statistics (Poisson errors) and fitting. And finally, we determine the number of standard deviations for the expected number of events to fluctuate up to the observed excess number of events.

		Expectation				
n	Observed	EW	Back.	Total	Excess	Number s.d.
0	126	20.2	25.1	45.3 $\pm$7.3	80.9	11.1σ
1	142		61.8	61.8 $\pm$9.5	80.2	8.4σ
2	148		104.2	104.2 $\pm$12.7	43.8	3.5σ

Table 18: The counting experiment for the opposite-side multiplicity between the jets using the fit with starting point of $n_0 = 3$ to determine the color-exchange background. For $n < n_0 = 3$ the table shows the observed number of events, the expected number of events from EW exchange and color-exchange, the error on this expectation, the excess number of events above the expectation, and the number of standard deviations for the expected number of events to fluctuate up to the observed number of events.

Table 18 shows the results using the multiplicity distribution between jets (i.e. Fig. 18(a)) and a fit starting point of $n_0 = 3$, while Table 19 corresponds to the multiplicity in $|\eta| < 1$ for a starting point of $n_0 = 2$. Clearly, on a bin-by-bin basis, electroweak exchange is significantly excluded, and the probability that the observed excess is due to the combination of electroweak color-singlet exchange and color-exchange background is much less than 10^{-10}.

		Expectation				
n	Observed	EW	Back.	Total	Excess	Number s.d.
0	219	20.2	59.5	79.6 ± 9.8	139.4	14.2σ
1	213		135.6	135.6 ± 13.7	77.4	5.7σ

Table 19: The counting experiment for the opposite-side multiplicity in the region $|\eta| < 1$ using the fit with starting point of $n_0 = 2$ to determine the color-exchange background. For $n < n_0 = 2$ the table shows the observed number of events, the expected number of events from EW exchange and color-exchange, the error on this expectation, the excess number of events above the expectation, and the number of standard deviations for the expected number of events to fluctuate up to the observed number of events.

To be conservative, we can also add the systematic error from the measurement of f_S to the total error on the observed excess. We note that this is not strictly correct, since varying the cuts and redoing a counting experiment is not the same as using the errors from varying the cuts and doing one counting experiment. Nonetheless, it does provide a conservative measure of the significance, given additional systematic uncertainty in the measurement. The systematic error in the zero bin is calculated by weighting the total systematic error by the excess in the zero bin: $7\% \cdot 81/205 = 3\%$. Adding in this systematic error gives a significance of 8σ for $n = 0$, which still corresponds to a probability of less than 10^{-10}.

		Expectation				
Region	Observed	EW	Back.	Total	Excess	Number s.d.
1	416	20	191	211 ± 26	205	8σ
2	432	20	195	215 ± 24	217	9σ

Table 20: The conservative counting experiment for the two opposite-side multiplicity distributions, which ignores bin-by-bin fluctuations.

We have also used another very conservative method that ignores bin-by-bin effects to determine the probability. Table 20 shows the results from both regions using the total number of expected events compared to the observed excess. Again, pure electroweak exchange is significantly excluded. Including the systematic error from the measurement ($7\% \equiv 16$ events) lowers the significance to about 7σ, which still corresponds to a probability of less than 10^{-10}.

14 Event Characteristics

We have plotted several quantities for events with $n_{cal} = 0$ (presumably color-singlet dominated) compared to all events. Figure 24 shows that the jet E_T and $\Delta\eta_c$ distributions are similar as might be expected, but the number of jets and $\Delta\phi$ distributions are significantly different. Events with $n_{cal} = 0$ typically have two reconstructed jets that are very back-to-back in ϕ, indicating that these events have little radiation, even in the forward region, consistent with expectations for color-singlet exchange.

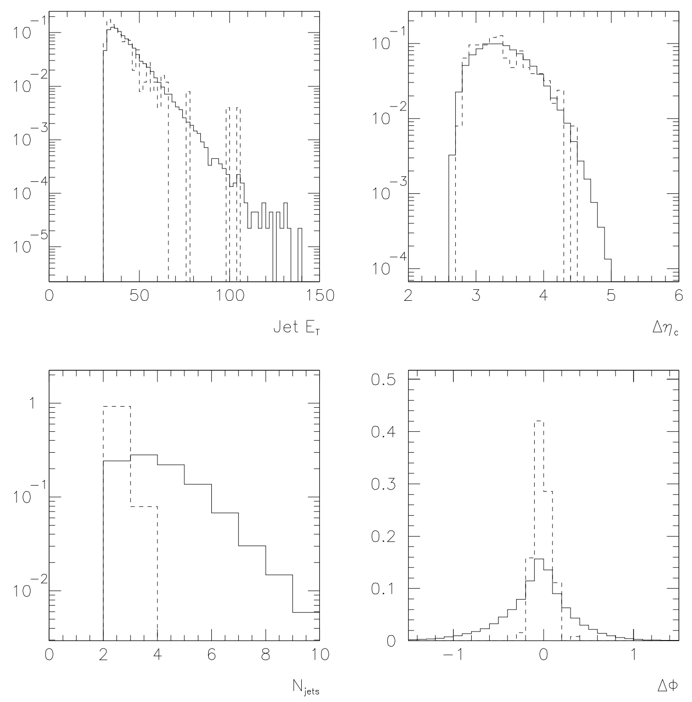

Figure 24: Comparison of events with $n_{cal} = 0$ to all events in the opposite-side sample. Shown are jet E_T spectrum (two leading jets), $\Delta\eta_c$, number of jets (above 8 GeV), and $\Delta\phi - \pi$.

15 Comparison of CDF and DØ Results

Our measurement of the fractional excess has a value and error similar to the Ref. [20] analysis mentioned in Sec. 3. We point out several differences between the two analyses.

1. The CDF data is based on a high E_T inclusive trigger ($E_T > 60$ GeV) and has little statistics for large rapidity intervals. The results are integrated over $\Delta\eta_c > 0.8$ and are thus dominated by the smaller $\Delta\eta_c$ points. The DØ sample on the other hand is for $\Delta\eta_c > 2.6$ which gives a significant reduction in the color-exchange background.

2. The CDF analysis fits the leading edge of the multiplicity distribution instead of the whole distribution, which may not be incorrect, but since this only gives them 8–10 points to determine the fit should involve larger uncertainties than they have quoted. We fit the whole distribution and have carefully taken into account all of the systematic errors including those from the fit parameters.

3. By plotting the track versus calorimeter results, we observe a clear excess without the aid of fits, while their excess is visually much less obvious.

4. We rigorously exclude electroweak exchange, while they simply state that "contributions from exchange of other colorless objects such as electroweak bosons are too small to explain our [their] result." Due to their higher background and errors which (in our opinion) have not been accounted for, they cannot quantitatively support this conclusion.

5. Their result likely includes some color-singlet events with low-multiplicity spectator interactions, which they do not discuss.

6. We also include the lower limit on the fraction of dijet events with a rapidity gap independent of survival probability.

We believe that our analysis represents a significant improvement over the CDF analysis.

The current CDF analysis [40] has a rapidity interval comparable to our analysis, but only about 5% of the number of events. They use the same-side jet multiplicity directly as the color-exchange background, which we feel is a suspect approach, especially as they may have some contamination from single diffractive jet events (which they do not reject at the trigger level). They obtain an excess of $2.0 \pm 0.7\%$ with no quoted systematic error.

16 Comparison to PRL Gap Fraction Result

In our previous publication [1], we plotted the rapidity gap fraction, which is defined experimentally as

$$f(\Delta\eta_c)^{exp} = \frac{N_{EM=0}(\Delta\eta_c)}{N(\Delta\eta_c)}.$$

This is the fraction of all events with no EM towers above 200 MeV between the leading jets. It should have a value near one for small jet separations, as nearly every event will have a rapidity gap, but is expected to decrease monotonically with increasing $\Delta\eta_c$ for color exchange, as fluctuations to zero multiplicity become unlikely. The solid circles in Fig. 25 show the published data. The flattening observed above $\Delta\eta_c = 2$ was indicative of color singlet exchange, but it was not definitively demonstrated that the flattening could not be due to inefficiencies or other detector effects. We now add the open circles, which are obtained from the value of NBD fits (for simplicity we use the single NBD) at $n_{\rm EM} = 0$ and represent the color-exchange background. While the fraction of events with $n_{\rm EM} = 0$ (solid circles) remains constant for $\Delta\eta_c > 2$, the value from the zero bin of the fit (open circles), which represents color-exchange, decreases rapidly. The difference between the two curves could be attributed to the portion of color-singlet exchange events which have no struck calorimeter towers between the jets. It should be noted that the upper limit of 1.1% only includes rapidity gap events which survive spectator interactions, while the excess above the fit measured earlier also includes those color-singlet events which have low multiplicity spectator interactions.

17 Conclusions

In conclusion, we have presented experimental evidence for strongly-interacting color-singlet exchange from a study of dijet events with $\Delta\eta_c > 2.6$ and jet $E_T > 30$ GeV. A striking enhancement of low-multiplicity events is observed independent of the details of the color-exchange background parameterization. The double NBD parameterization provides a measurement of the color-exchange background and confirms that this background was small for the rapidity gap fraction previously measured in Ref. [1]. The fractional excess above the color-exchange background is measured to be $(1.07 \pm 0.10(\text{stat})^{+0.25}_{-0.13}(\text{syst}))\%$ which is consistent with the presence of strongly-interacting color-singlet exchange and inconsistent with electroweak exchange.

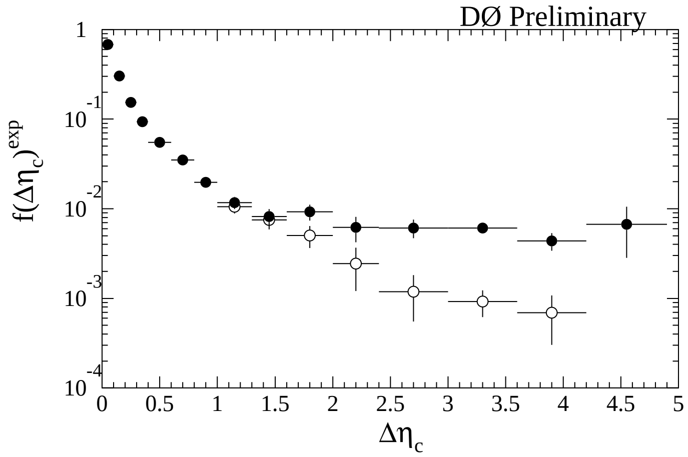

Figure 25: The fraction of events that have no tagged particles between the two leading jets (solid circles) and the value of the negative binomial fit for the zero multiplicity bin (open circles) as a function of $\Delta\eta_c$. The error bars show the statistical uncertainty only.

References

[1] S. Abachi *et al.* (DØ Collaboration), Phys. Rev. Lett. 72, 2332 (1994).

[2] B. May, Ph.D. Dissertation, University of Arizona (1994) (unpublished).

[3] Y. Dokshitzer, V. Khoze and S. Troyan, "Proceedings of the 6th International Conference on Physics in Collisions" (1986), ed. M. Derrick, 417 (World Scientific, Singapore, 1987);
Y. Dokshitzer, V. Khoze and T. Sjöstrand, Phys. Lett. **B274**, 116 (1992).

[4] J. D. Bjorken, Phys. Rev. D**47**, 101 (1992).

[5] R. S. Fletcher and T. Stelzer, Phys. Rev. D**48**, 5162 (1993).

[6] H. Chehime and D. Zeppenfeld, MAD/PH/814 (1994).

[7] F. Low, Phys. Rev. **D12** 163 (1975);
S. Nussinov, Phys. Rev. **D14** 246 (1976);

N. Nikolaev and B. Zakharov, DFTT-5/91 (1991) and references therein;
E. Berger, J. Collins, G. Sterman and D. Soper, Nucl. Phys. **B286**, 704 (1987).

[8] Ya. Balitsky and L. Lipatov, Sov. J. Nucl. Phys. **28**, 822 (1978);
L. Lipatov, Sov. Phys. JETP **63**, 904 (1986).

[9] V. Del Duca and W. K. Tang, *Proceedings of the 5th Blois Workshop on Elastic and Diffractive Scattering* (1993), ed. H.M. Fried, K. Kang, and C.-I. Tan, (World Scientific 1994).

[10] H. Chehime *et al.*, Phys. Lett. B **286**, 397 (1992).

[11] E. Gotsman, E. M. Levin and U. Maor, Phys. Lett. B **309**, 199 (1993).

[12] H. Bengtsson and T. Sjöstrand, Comput. Phys. Commun. **46**, 43 (1987).

[13] G. Marchesini and B.R. Webber, Nucl. Phys. **B310**, 461 (1988).

[14] R. Bonino *et al.* (UA8 Collaboration), Phys. Lett. **B211**, 239 (1988).

[15] A. Brandt *et al.* (UA8 Collaboration), Phys. Lett. **B297**, 417 (1992).

[16] A. Brandt *et al.* (UA8 Collaboration), Nucl. Instrum. and Meth. in Phys. Res. **A327** 412 (1993).

[17] ZEUS Collab., M. Derrick et al., Phys. Lett. **B332** (1994) 228.

[18] ZEUS Collab., M. Derrick et al., Phys. Lett. **B346** (1995) 399.

[19] H1 Collab., T. Ahmed et al., Nucl. Phys. **B435** (1995) 3.

[20] F. Abe *et al.* (CDF Collaboration), Phys. Rev. Lett. **74**, 855 (1995).

[21] R. Fletcher, "Multiplicity between Jets in PYTHIA56" (1994) (unpublished).

[22] E. Levin, private communication.

[23] G. Alner *et al.* (UA5 Collaboration), Phys. Rep. **154**, 247 (1987).

[24] I. Sarcevic and B. Fletcher, private communication.

[25] P. Abreu *et al.* (DELPHI Collaboration), Z. Phys. C52, 271 (1991); Z. Phys. C56, 63 (1992).

[26] A.D. Martin and C.J. Maxwell, Z. Phys. C34, 71 (1987).

[27] C.S. Kim, Z. Phys. C51, 619 (1991)

[28] I. Dremin, submitted to Physics Uspekhi, FIAN TD-6, (1994) and references therein.

[29] K. Goulianos, FERMILAB-Conf-94/266-E (1994).

[30] A. Giovaninni, S. Lupia and R. Ugoccioni, DFTT 28/94 (1994)

[31] J. Cugnon and O. Harouna, Europhys. Lett. 4, 1127 (1987).

[32] E. Malaza and B. Webber, Nucl. Phys. **B267**, 702 (1986)

[33] B. Andersson, P. Dahlqvist and G. Gustafson, Phys. Lett. **B214**, 604 (1988).

[34] K. Fialkowski, B. Wosiek and J. Wosiek, Acta Phys. Pol. **B20**, 639 (1989);

[35] B. Flannery et al.. "Numerical Recipes in FORTRAN" (1992).

[36] J. Pumplin Phys. Rev. **D50**, 6811 (1994).

[37] A. Jonckeere, "Proceedings of the Argonne National Laboratory Detector Simulation Workshop" (1987); DØNote 638 (1987) (unpublished).

[38] J. Bantly, Q. Li-Demarteau, 'Multiple Interaction Tool', DØNote 1691;
J. Bantly, 'Multiple Interaction Tool Study', DØNote 1849.

[39] A. Brandt, *Proceedings of the 27th International Conference on High Energy Physics*, (1994), ed. P. J. Bussey, I.G. Knowles (Institute of Physics Publishing, Bristol, 1995).

[40] P. Melese (CDF Collaboration) *Proceedings of the QCD and High Energy Interaction XXXth Moriond Conference*, Les Arcs, France, March 19-26, 1995.